RSC Advances

PAPER

View Article Online
View Journal | View Issue

Cite this: *RSC Adv.*, 2025, **15**, 48585

Carrageenan grafted with acrylic acid and sulfonamide induces apoptosis and suppresses proliferation in A549 lung cancer cells: synthesis, cytotoxicity, gene expression, and *in silico* studies

M. S. Hashem, *[a] Asmaa M. Fahim *[b] and Ghada H. Elsayed [cd]

This study was aimed at developing an effective, low-cost, safe, and selective anticancer agent through a free radical-triggered grafting copolymerization process of carrageenan with acrylic acid (AA) and sulfonamide derivative (Br-PS) in good yield. The resulting product, poly(Br-PS-*co*-AA)-*g*-carrageenan, was subjected to energy dispersive X-ray (EDX) spectroscopy, scanning electron microscopy (SEM), thermal gravimetric (TG) analysis, and Fourier-transform infrared (FT-IR) spectroscopy for its characterization. Compared with doxorubicin (IC_{50} = 16.1 μg/mL; SI = 9.1), poly(Br-PS-*co*-AA)-*g*-carrageenan exhibited a stronger growth inhibition and higher selectivity against A549 cells with IC_{50} = 12.3 μg/mL and SI = 11.7 after 48 hours, as assessed by the neutral red uptake assay. Meanwhile, gene expression analysis revealed that treatment with poly(Br-PS-*co*-AA)-*g*-carrageenan decreased the expression levels of C-myc and Cyclin D1 while elevating P21 levels in A549 cells, thereby suppressing cell proliferation and promoting apoptosis. Furthermore, the electronic and structural properties of poly(Br-PS-*co*-AA)-*g*-carrageenan were validated through density functional theory (DFT) calculations. Molecular docking and dynamic simulations demonstrated a potent affinity for binding to important cancer-related targets, such as EGFR, C-myc, and P21, with stable conformational dynamics. The study concludes that poly(Br-PS-*co*-AA)-*g*-carrageenan is a safe, effective, and promising option for treating lung cancer that merits more preclinical research.

Received 30th October 2025
Accepted 20th November 2025

DOI: 10.1039/d5ra08332j

rsc.li/rsc-advances

1. Introduction

Carrageenans are natural galactans that are extracted from red seaweed and can be used as medicinal excipients owing to their excellent biomedical activity, biocompatibility, biodegradability, thermostability, hydrophilicity, and non-toxicity.[1,2] One significant benefit of carrageenan is the large number of hydroxyl groups that are readily available in its chain. This is primarily influenced by a chemical change that has been suggested to alter its physiological chemical characteristics for biological uses.[3,4] Carrageenans are categorized into three main types based on the sulfate group numbers per disaccharide unit, as well as their position, in addition to the degree of sulfation: κ-carrageenan possesses one sulfate group, ι-carrageenan has two sulfate groups, and λ-carrageenan comprises three sulfate groups.[5,6] In the carrageenan family, iota-carrageenan, an anionic water-soluble polysaccharide with 15–40% of ester sulfates, is utilized in biomedical, food, and pharmaceutical applications as an emulsifier, hydrophilic gelling agent, hydrocolloidal carrier, thickener, and viscosifier since it forms soft gels that are appropriate for topical delivery and wound dressing.[7–9] Additionally, it shows excellent antibacterial, antitumor, anti-inflammatory, antiviral, and immunomodulatory activities.[10,11]

To develop biological activity as an anticancer agent, iota-carrageenan needs to be modulated to augment its efficiency, hydrophilicity, selectivity, and sensitivity characteristics. Accordingly, various synthetic polymeric materials, such as polyacrylic acid and polyacrylamide, have been grafted onto the carrageenan skeleton.[12–14] Furthermore, grafting copolymerization with various polymeric materials, such as sulfonamide derivatives, could result in the incorporation of amide groups and extra sulfate groups. These functional categories are believed to help increase the potential anticancer activity of carrageenan.

Lung cancer is the leading cause of cancer-related fatalities worldwide, with 5-year survival rates ranging from 4% to 17% based on stage and geographical differences.[15] One important

[a]*Polymers and Pigments Department, National Research Centre, Dokki, Giza 12622, Egypt. E-mail: ms.hashem@nrc.sci.eg*

[b]*Department of Green Chemistry, National Research Centre, Dokki, Giza 12622, Egypt. E-mail: asmaamahmoud8521@gmail.com*

[c]*Hormones Department, Medical Research and Clinical Studies Institute, National Research Centre, Dokki, Giza 12622, Egypt*

[d]*Stem Cell Lab, Centre of Excellence for Advanced Sciences, National Research Centre, Dokki, Giza 12622, Egypt*

factor that induces carcinogenesis is the C-myc oncoprotein. In healthy cells, transcriptional and post-transcriptional processes closely regulate the C-myc expression. Lung, breast, and colon cancers are among the more than half of human malignancies that activate C-myc by chromosomal translocations, gene amplification, or insertional mutagenesis.[16] The potent oncogenic role of C-myc has been extensively demonstrated in both murine models and cell culture systems.[17] C-myc functions as a transcription factor that may transcriptionally control the expression of target genes in conjunction with its partner protein Max.[18] Previous studies have suggested that C-myc directly regulates 10–15% of genomic genes, while more recent findings indicate that it acts as a global amplifier of existing promoters.[19] C-myc controls several cellular functions, such as cell division, proliferation, metabolism, and genomic instability, by altering the expression of target genes.[20] Another key regulator is P21, also known as cyclin-dependent kinase inhibitor 1A (CDKN1A) or P21Waf1/Cip1, is crucial for controlling cell division and preserving genomic integrity.[21] In response to a variety of stimuli, including oncogene-induced proliferation, it can cause G1 arrest and cell senescence.[22] Beyond its canonical role in cell cycle arrest, P21 has been applied in modulating drug resistance and proliferation in cancer cells.[23] Cyclin D1, a key regulator of the G1 phase, is frequently overexpressed in a wide range of tumors largely due to oncogenic signaling pathways.[24,25] By accelerating the cell cycle's transition from the G1 to S phases and enhancing its regulatory role, overexpression of this gene may serve as an oncogenic stimulus.[26] In accordance with Ramos-Garcia *et al.*,[27] overexpression of Cyclin D1 is a significant molecular alteration in several malignancies that predicts prognostic and clinicopathological importance.

The current research aimed to structure an inventive, safe, effective, selective, and low-cost anticancer agent based on carrageenan grafting with a copolymer composed of AA and Br-PS, which was verified through FT-IR, EDX, and SEM. We examined the cytotoxic effect of carrageenan and poly(Br-PS-*co*-AA)-*g*-carrageenan against the human lung cancer cell line A549 and the normal Madin–Darby Canine Kidney cell line MDCK. In addition, we evaluated the mRNA expression levels of C-myc, P21, and Cyclin D1 in A549 cells, which supports the findings through theoretical DFT calculations and molecular docking simulations against key cancer-related targets.

2. Experimental section

2.1. Materials

ι-Carrageenan (type two, commercial quality, and majority iota carrageenan) was purchased from Sigma. Acrylic acid (AA, <99%) was obtained from Merck and filtered using an alumina column to eliminate the hydroquinone. The source of ammonium peroxydisulfate (APS, 99%) was BDH. A novel monomeric sulfonamide derivative, (*E*)-*N*-(4-(3-(4-bromophenyl)acryloyl) phenyl)-4-methylbenzene sulfonamide (Br-PS), was manufactured and evaluated in line with an earlier report.[28] Water with double distillation (DDW) was prescribed for all solution production in this investigation.

2.2. Characterization

The Shimadzu FT-IR 8101 PC infrared spectrophotometer recorded the IR spectra. Energy dispersive X-ray analysis (EDX) alongside scanning electron microscopy (SEM) shots originated with JEOL-JSM-6390LV. The thermal analyses were carried out using a Shimadzu DTG-60 simultaneous thermal analyzer with a flow of nitrogen (50 mL min^{-1}). Approximately 10 mg of the dried sample was heated from 25 to 800 °C at a constant heating rate of 10 °C min^{-1}. Weight loss and heat-flow curves were analyzed using TA Universal Analysis software.

2.3. Poly(Br-PS-*co*-AA)-*g*-carrageenan structurization

Poly(Br-PS-*co*-AA)-*g*-carrageenan was synthesized using the grafting copolymerization method induced by free radicals, utilizing APS as the initiating agent. 0.5 g of carrageenan was dissolved in 40 mL of DDW by stirring, along with heating at 50 °C. Thereafter, the dissolved carrageenan was sonicated with 0.05 g of Br-PS whenever completely suspended. Then, the suspended mixture was carried to the reaction system composed of a one-hundred-mL triple-necked flask comprising a condensing tube, nitrogen inlet, in addition to a thermometer. The polymerization process began and continued for 4 hours after adding 0.075 g of APS dissolved in 10 mL of DDW, followed by 1 mL of AA under a magnetic stirrer at 70 °C. The stable emulsion formed was placed over a Petri dish containing hot DDW to eliminate any remaining traces of unreacted carrageenan. The composite was soaked in both acetone and ethanol for about seven days to get rid of homopolymers or unpolymerized monomeric materials. Following collection, the grafted carrageenan composite was permitted to air-dry for one day at around 40 °C prior to storing at ambient temperature, awaiting analysis and conceivable uses.

2.4. Grafting degree percentage determination

The carrageenan grafting degree (GD) percentage with poly(Br-PS-*co*-AA) was determined by the carrageenan weights prior to and post the grafting copolymerization operation based on the following equation:[29,30]

$$\mathrm{GD}(\%) = \frac{W_a - W_b}{W_b} \times 100,$$

where W_b and W_a are the weights of carrageenan prior to and post-grafting copolymerization.

2.5. DFT investigation

Utilizing the Gaussian 09W program,[31] the theoretical studies were performed using the DFT/B3LYP/6-31 basis set level, relying on the Berny method.[32,33] Symmetry constraints were not implemented during the optimization of geometry.[34] The wide-ranging vibrational modes were assigned using the potential energy distribution (PED), determined by the vibrational energy distribution analysis (VEDA) program.[35]

2.6. Biological activity analysis

2.6.1. Cytotoxic neutral red uptake assay. After being acquired from the American Type Culture Collection (ATCC), the A549 and MDCK cell lines were maintained under optimal conditions. A549 and MDCK cells were cultivated at 37 °C in 5% CO_2, humidified in DMEM (Dulbecco's modified Eagle's Medium) supplemented with 10% fetal bovine serum (FBS), 100 U/mL penicillin, and 100 μg/mL streptomycin sulfate. Trypsin–EDTA was used to disintegrate the cells and pass them. The experiment employed cells in the logarithmic growth phase. According to Repetto *et al.*,[36] the *in vitro* neutral red absorption test was used to evaluate cytotoxicity. In brief, cells were seeded at a density of 1×10^4 cells per well and treated for 48 hours with 25, 50, 100, and 200 μg/mL of the compounds studied. After incubation, all wells were filled with 100 μL of 0.4 μg/mL neutral red working solution (Sigma-Aldrich, Germany), which was then incubated for 2 h at 37 °C. Using a microtiter plate reader spectrophotometer (Sorin, Biomedica S.p.A., Milan, Italy), the neutral red color intensity of the extract was measured at 450 and 630 nm as excitation and emission wavelengths. The half maximum inhibitory concentration (IC_{50}) of the investigated compounds is determined by the relationship between the neutral red intensity value and the utilized log concentrations. The examined compounds were substituted with medium for the untreated cells (negative control). A 100% inhibition was achieved using doxorubicin, a cytotoxic natural substance (Mr = 543.5), as a positive control. After dissolving these compounds in dimethyl sulfoxide (DMSO), the final concentration on the cells was less than 0.2%. Every test was conducted at least 3 times. In comparison to the control, the percentage of cell growth was computed as follows:

$$\%\ \text{Cell growth} = (\text{absorbance of compounds/absorbance of control}) \times 100$$

2.7. Selectivity index (SI)

The selectivity index (SI), calculated by the analyzed compound's IC_{50} in normal cells against cancer cells, demonstrates the cytotoxic selectivity (*i.e.*, safety) of the studied compounds towards cancer cells as opposed to normal cells.[37]

2.8. Quantitative real-time PCR (qRT-PCR) analysis

The RN easy mini-Kit (Qiagen, Germany) (Cat. No.: 74104) was used to separate RNA from A549 cells (3×10^4 cells per well) after they had been treated for 48 hours. A NanoDrop 2000 spectrophotometer (Thermo Fisher Scientific, USA) was used to measure the concentration and purity of the extracted RNA. The 260/280 nm absorbance ratio was utilized to assess the quality of the RNA. Using the Revert Aid First Strand cDNA Synthesis Kit (Thermo Fisher Scientific, USA) (Cat. No.: K1621), the RNA from each treatment was transformed into first-strand cDNA in accordance with the manufacturer's instructions. In Table 1, certain primer sequences are mentioned. Using the Maxima SYBR Green qPCR Master Mix (2X) (Thermo Fisher Scientific, USA) (Cat. No.: K0221), the expression levels of the C-myc, P21, and Cyclin D1 genes were normalized with respect to the β-Actin transcript and computed using the $2^{-\Delta\Delta CT}$ technique.[38] The following reaction conditions were used: 40 cycles of amplification at 95 °C for 10 minutes, 95 °C for 15 seconds, 60 °C for 30 seconds, and 72 °C for 30 seconds. To determine gene expression, the DNA Technology Detecting Thermocycler DT Lite 4S1 (Russia) was used.

2.9. Statistics

Data are presented as mean ± SEM (standard error of the mean). Version 11 of the Sigma Plot was utilized to analyze the data. The Student's *t*-test was employed to analyze the data and identify any significant differences between the studied compounds. Statistical significance was defined as $p < 0.05$. Each set of data could be replicated.

2.10. Docking simulation

All molecular docking studies for this research were carried out using the Molecular Operating Environment (MOE) and AutoDock Vina modules integrated into Discovery Studio Client v4.2.[41,42] All receptor structures were obtained from the Protein Data Bank (PDB) and prepared for molecular docking trials by removing water molecules and co-crystallized ligands, adding polar hydrogens, and geometry optimizing side-chain complexes using the AMBER/CHARMM force field. Subsequent to receptor preparation, the ligands involved in the study (*i.e.*, carrageenan, poly(Br-PS-*co*-AA)-*g*-carrageenan, and doxorubicin) were geometry optimized before docking using two procedures at the DFT/B3LYP/6-31G level (in computational chemistry), and acceptable docking methods applicable to those ligands. Molecular dockings were executed with a cubic grid box ($60 \times 60 \times 60$ Å^3) employing a grid spacing of 0.375 Å, with the center of the box being on each native ligand binding pocket. Ten docking runs were conducted per ligand with docking energy ranges and a threshold to convergence defined at 3 kcal mol^{-1} and an RMS gradient of 0.01. The docking plus epidermal growth factor receptor tyrosine kinase domain with

Table 1 List of the primers for qRT-PCR

Gene	Primer forward (5′-3′)	Primer reverse (5′-3′)	References
β-Actin	CCTTCCTGGGCATGGAGTCCT	GGAGCAATGATCTTGATCTTC	39
C-myc	AGAGAAGCTGGCCTCCTACC	CGTCGAGGAGAGCAGAGAAT	40
P21	AAGACCATGTGGACCTGT	GGTAGAAATCTGTCATGCTG	39
Cyclin D1	GAGGAAGAGGAGGAGGAGGA	GAGATGGAAGGGGGAAAGAG	39

4-anilinoquinazoline inhibitor erlotinib (PDBID: 1M17),[43] crystal structure of MS0802, c-Myc-1 binding protein domain from *Homo sapiens* (PDBID: 2yy0),[44] and structure of the 16S rRNA methylase RmtB, P21(PDBID: 3RFH).[45] Additionally, EGFR (PDB ID 1M17), C-myc (PDB ID 2yy0), and P21 (PDB ID 3RFH) were selected because they all serve as key regulators in lung cancer progression. EGFR is a tyrosine-kinase receptor overexpressed in A549 cells, and the inhibition of EGFR suppresses tumor proliferation and survival signals. C-myc is an oncogenic transcription factor that regulates cell cycle genes, and P21 (CDKN1A) is a tumor-suppressor protein whose activation brings about growth arrest and apoptosis. These three proteins allow for a more direct mechanistic correlation of the *in vitro* gene expression data presented in this study, which clearly documents down-regulation of C-myc and up-regulation of P21 transcripts. Ten distributed docking simulations were conducted using the standard parameters. Conformations were created according to the *E* conformation, the overall data organization, together with the proper positioning of pertinent amino acids in each protein's linkage pocket.[46] Molecular dynamics simulation of the investigated materials was performed through GROMACS[47] in water with AMBER/CHARMM alongside polymer-specific factors at 300 K. Conformations identified or calculated with the lowest-energy binding energies from a scoring function of the MD and/or docking software were inspected for the assessment of interactions involving hydrogen bonds and hydrophobic contacts, as viewed in Discovery Studio. To justify all binding poses, short-time energy minimization and re-scoring were performed.

3. Results and discussion

3.1. Grafting copolymerization with a poly(Br-PS-*co*-AA)-*g*-carrageenan structure

Free radical-triggered grafting copolymerization is a well-established technique for enhancing composites.[48,49] Copolymerization of Br-PS and AA monomeric materials on the carrageenan skeleton was achieved depending on the ammonium peroxydisulfate decomposition upon heating, resulting in sulfate radicals, which removed hydrogens of hydroxyl groups within the carrageenan skeleton, generating corresponding alkoxy macro-initiator radicals.[50,51] The interaction between carrageenan and APS led to a series of redox reactions that produced new active centers that rapidly initiated monomeric materials, leading to poly(Br-PS-*co*-AA)-*g*-carrageenan formation, as illustrated in Scheme 1. The percentage of poly(Br-PS-*co*-AA) grafting degree (GD%) upon the carrageenan backbone was 66.5% ± 0.5%, confirmed by the initial weight of carrageenan and its weight resulting from the grafting copolymerization reaction. Poly(Br-PS-*co*-AA)-*g*-carrageenan has two possible pathways concerning Scheme 1. Consistent with the postulated structure (1), the alkoxy macro-radical generated in the D-galactose portion from one unit of carrageenan could target the double bonds within the monomeric materials. Further, the olefinic groups inside Br-PS and AA could be attacked by the alkoxy macro-radical manufactured at the D-galactose sections from two units of carrageenan, as per the hypothesized structure (2).

3.2. FT-IR investigation

The main characteristic peaks of native carrageenan, Br-PS, plus poly(Br-PS-*co*-AA)-*g*-carrageenan were verified through Fourier transform infrared (FT-IR) spectroscopy within wavenumbers ranging from 400 to 4000 cm^{-1} (Fig. 1(a–c)). The spectrum graph of carrageenan in Fig. 1 showed a stretching broad band of O–H (3390–3180 cm^{-1}) indicative of OH groups, stretching bands of C–H (2970–2900 cm^{-1}) according to the carbohydrate skeleton, and notable SO_3 group stretching bands (1225–1037 cm^{-1}) owing to the asymmetric and symmetric stretching of OSO_3.[52] The emerged bands at 804–843 cm^{-1} and 970 cm^{-1} indicate the additional C–O–SO_3 that is only found in ι-carrageenan.[53,54] The grafting copolymerization of AA and Br-PS upon carrageenan was ascertained through variations between the spectral FT-IR for carrageenan and Br-PS, in addition to the grafting copolymeric one. Fig. 1(c) depicts the overlapping of the distinctive bands of Br-PS and carrageenan with each other, as well as a minimal shift. Asymmetrical stretching at 1187 cm^{-1} and 1410 cm^{-1} with the intense symmetrical bands on account of the S=O groups, confirmed grafting polymerization. The sharp band around 3209 cm^{-1} with a wide band in the vicinity of 3350–3150 cm^{-1} was attributed to the overlap between the OH groups from AA and carrageenan and the N–H stretching group bands from the sulfonamide derivative. Additionally, the bands close to 1720 cm^{-1} and 1657 cm^{-1} corresponded to the bending vibrations of C=O from AA and N–H from Br-PS, respectively.[55] The presence of distinct bands of carrageenan, sulfonamide derivative, as well as those of acrylic acid, emphasized the grafting process involving Br-PS copolymerized with AA upon the carrageenan skeletal.

3.3. SEM analysis

Morphological screening was studied using scanning electron microscopy (SEM), including a thin gold layer applied to the samples as a coating. Native carrageenan (Fig. 2(a)) showed a compact surface with wrinkled layers; with magnification, the surface appeared smooth, and some parts were cloudy and smoky (Fig. 2(b)). However, after grafting copolymerization with Br-PS and AA, the carrageenan surface had some porosity and was covered with upper cluster layers of the grafting copolymer, as shown in Fig. 2(c). When these clusters were magnified, it was noticed that their pieces had cubical shapes, as illustrated in Fig. 2(d). These images and observations proved the grafting process of poly(Br-PS-*co*-AA) and its distribution on the carrageenan surface. Energy-dispersive X-ray (EDX) spectroscopy analysis investigated the elemental composition with reference to carrageenan, together with poly(Br-PS-*co*-AA)-*g*-carrageenan. The EDX spectra of carrageenan indicate the presence of C, O, and S; however, the EDX spectra for poly(Br-PS-*co*-AA)-*g*-carrageenan contained C, O, N, S, and Br, which indicated successful poly(Br-PS-*co*-AA)-*g*-carrageenan synthesis.

3.4. Thermogravimetric and differential thermal analyses (TG/DTG)

The TG and DTG curves demonstrated a multi-stage degradation profile typical of sulfated carrageenan. The first small

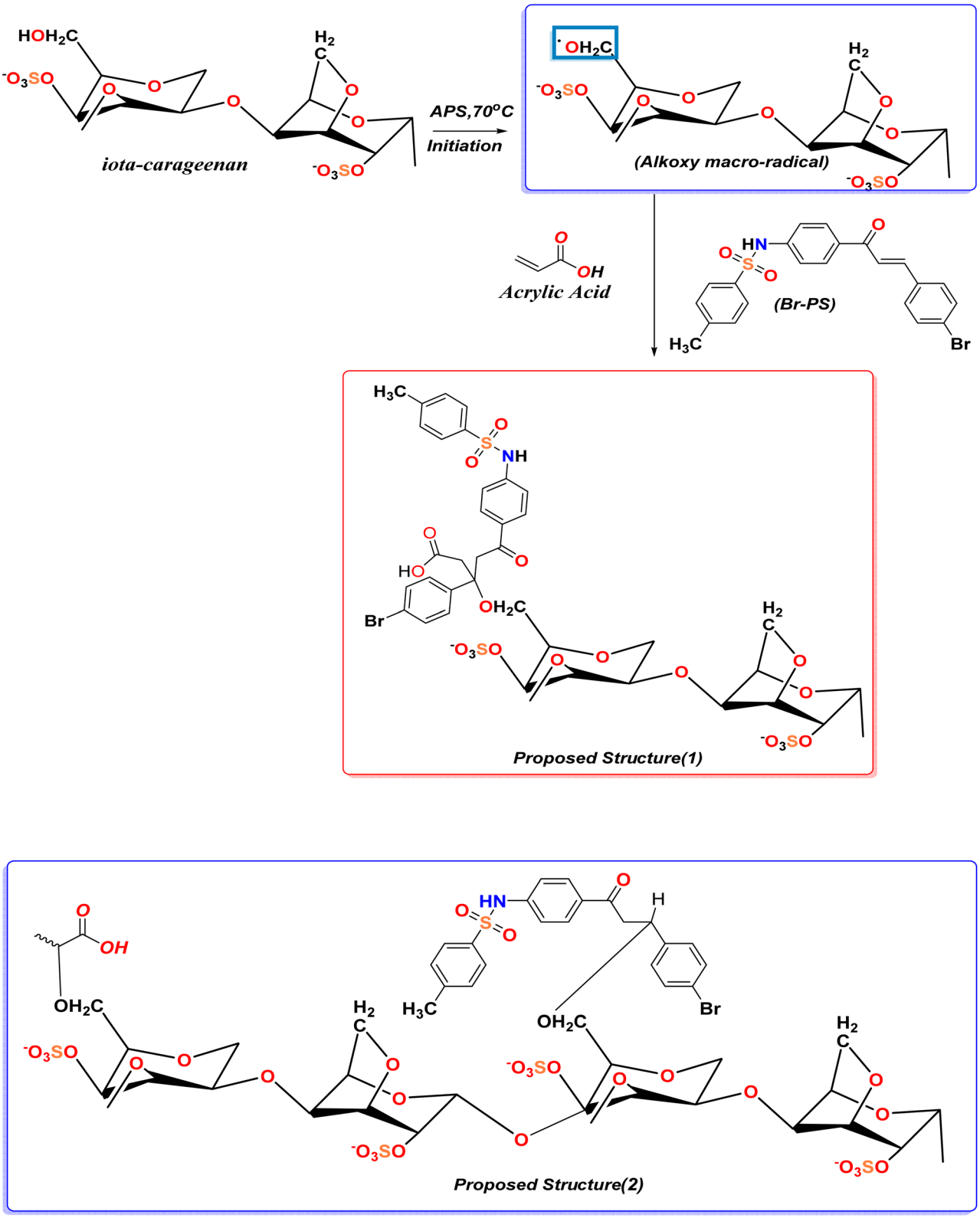

Scheme 1 Poly(Br-PS-*co*-AA)-*g*-carrageenan synthesis and its proposed structures.

weight loss (~8%) below 120 °C correlated to the evaporation of moisture that was physically adsorbed on carrageenan, and there was an endothermic peak. Most of the mass loss (200–420 °C, ~60%) occurred due to desulfation and depolymerization of the glycosidic backbone, with evidence of broad endothermic signals in the range of 260–350 °C. A small exothermic

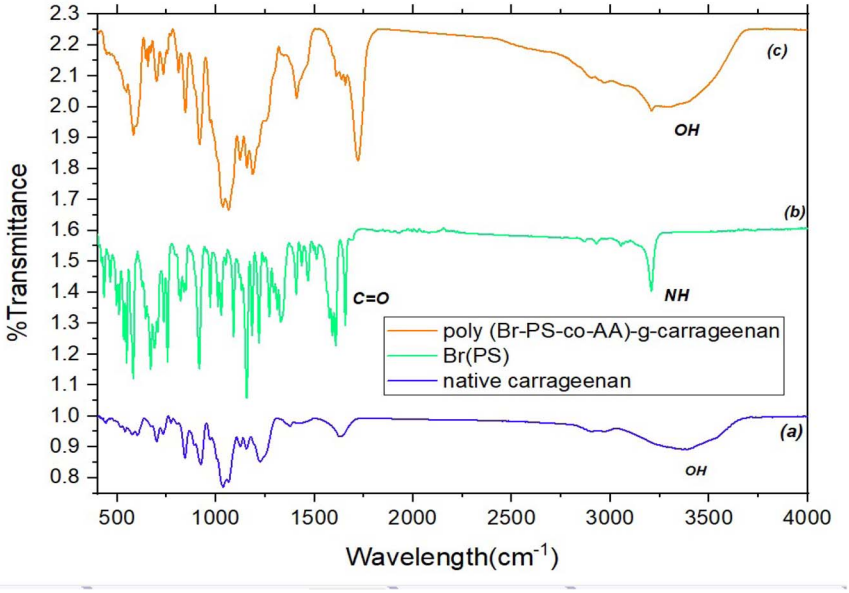

Fig. 1 FT-IR spectra for (a) native carrageenan, (b) Br-PS, and (c) poly(Br-PS-*co*-AA)-*g*-carrageenan.

event around 520 °C corresponded to the rearrangement and carbonization of the residual char. The residue (~20%) corresponded to a carbonaceous matrix that was thermally stable at high temperatures. Overall, carrageenan was thermally stable up to ~220 °C, consistent with its robust polysaccharide structure. The TG and DTG thermal profiles (Fig. 3) provided insights into the thermal modal behavior along with the thermal stability parameters of the poly(Br-PS-*co*-AA)-*g*-carrageenan in a nitrogen environment. The small upfront weight loss (≈5%) before 120 °C corresponded to moisture desorption as well as the loss of volatiles that were adhered to the polymer surface. The TG curve of a simplified (two-step) behavior for poly(Br-PS-*co*-AA)-*g*-carrageenan is due to uniform grafting and a lower number of labile sulfate groups compared to neat carrageenan. Grafting poly(Br-PS-*co*-AA) reduces both random desulfation and thermal decomposition mechanisms connected to moisture, resulting in a more distinct degradation event from 280 to 460 °C. Neat carrageenan, however, undergoes multiple overlapping mechanisms for desulfation and depolymerization that yield a multi-step TG profile. The higher percentage of residual carbon (~25%) also supports an assessment of greater aromaticity, as well as a degree of carbonization with increased temperature, in agreement with the EDX evidence of Br, N, and S incorporation. The accompanying weight loss stage represented degradation of the polysaccharide backbone and sulfonamide-grafted units and occurred in the larger loss interval at approximately 280–460 °C. The step nature of this degradation contributed to the overall weight loss in the DTG and to the resolution of the change in the DTG curve. In principle, an acute change in DTG indicates the resolution of a degradation event common to any experimental method governing a chemically bonded nature. A final gradual weight loss above 600 °C demonstrated a carbonization effect, creating a stable aromatic char that formed about 25% of the original weight. The elevated temperature and significant char yield confirmed the thermal resistance imparted by the rigid sulfonamide unit through improved interactions, as well as π–π stacking between potentially neighboring aromatic segments. Therefore, a mechanistic description based on the chemical structure and known literature on aromatic graft copolymers suggests that the higher temperature of decomposition may be because of aromatic sulfonamide units from the Br-PS moiety, imparting π–π stacking and limiting the mobility of the polymer chains. Additionally, the quantitative comparison illustrates that grafting causes T_{onset} and T_{50} to shift to higher temperatures, indicating that the grafted copolymer possesses greater thermal stability due to greater crosslinking and the introduction of aromatic substitution derived from the acrylic acid and Br-PS moieties, respectively, as displayed in Table 2.

3.5. Computational analysis

3.5.1. Optimization of the proposed structure. In this study, we optimized the structures that were suggested for poly(Br-PS-*co*-AA)-*g*-carrageenan using Gaussian (09)[31,56–58] by means of DFT/B3LYP/6-31(G) basis set. Additionally, the physical descriptors of optimized proposed structure (1 and 2) were concerning on absolute hardness (η),[59] electronegativities (χ),[60] absolute softness (σ),[61] chemical potential (P_i),[62] global softness (S),[63] global electrophilicity (ω),[64] and electronic charge (ΔN_{max}),[65] regarding the equations from (1)–(8) intended in Table 2 alongside with Fig. 3(A–C).[55,66,67]

$$\Delta E = E_{LUMO} - E_{HOMO} \quad (1)$$

$$\chi = \frac{-(E_{LUMO} + E_{HOMO})}{2} \quad (2)$$

$$\eta = \frac{(E_{LUMO} - E_{HOMO})}{2} \quad (3)$$

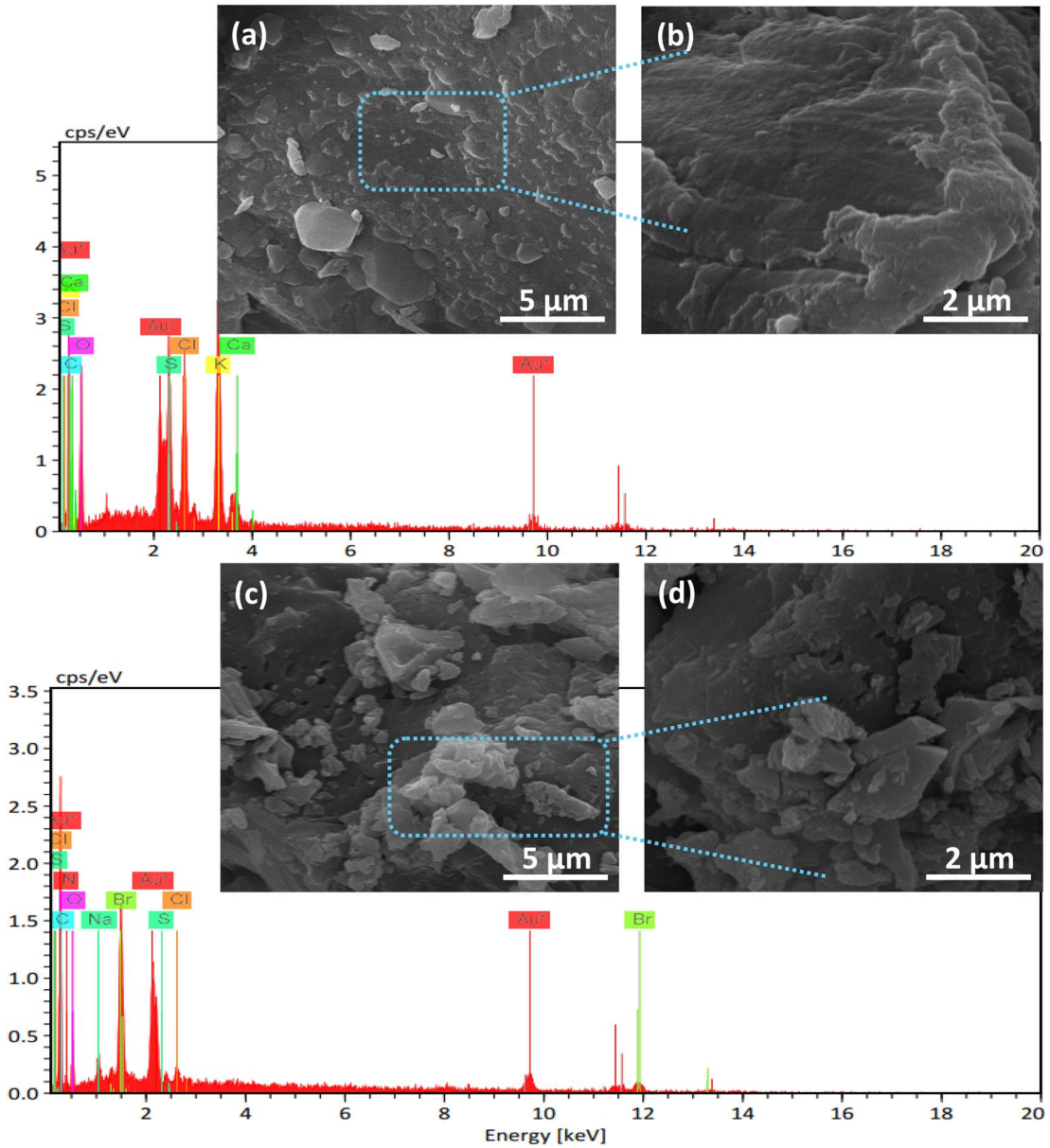

Fig. 2 SEM images and EDX spectra of (a and b) native carrageenan and (c and d) poly(Br-PS-*co*-AA)-*g*-carrageenan.

$$\sigma = 1/\eta \quad (4)$$

$$P_i = -\chi \quad (5)$$

$$S = 1/2\eta \quad (6)$$

$$\omega = P_i^2/2 \quad (7)$$

$$\Delta N_{max} = -P_i/\eta \quad (8)$$

The optimization of the two proposed structures using B3LYP/6-31(G) basis set was non-planar, as depicted in Fig. 4(Aand B), with their physical descriptor (Table 3), and the two structures showed the presence of one unit of carrageenan or two units of carrageenan, which interact with Br-PS and acrylic acid. The proposed structure 1 manifested a total energy of −65259.1934 eV, which is less stable than structure 2 with −108412.6626 eV, which is more stable due to the stronger electronic interaction. Additionally, the displayed HOMO–LUMO gap energy for the proposed structure 1, with a high gap energy of about 1.25 eV, was less reactive and more kinetically stable (hard structure), and its HOMO = −7.954 eV (good nucleophile) and LUMO = −6.701 eV (moderate electron acceptor), as demonstrated in Fig. 4(A). The proposed structure 2 showed a very narrow gap with 0.096 eV, which is highly reactive, has softness properties, and its HOMO = −0.069 eV/LUMO = 0.026 eV (highly polarizable) (Fig. 4(B)). The electronegativity of proposed structure 1 showed a higher χ (7.327 eV) with a strong tendency to attract electrons, and proposed structure 2 was approximately zero with 0.021 eV, which is a low

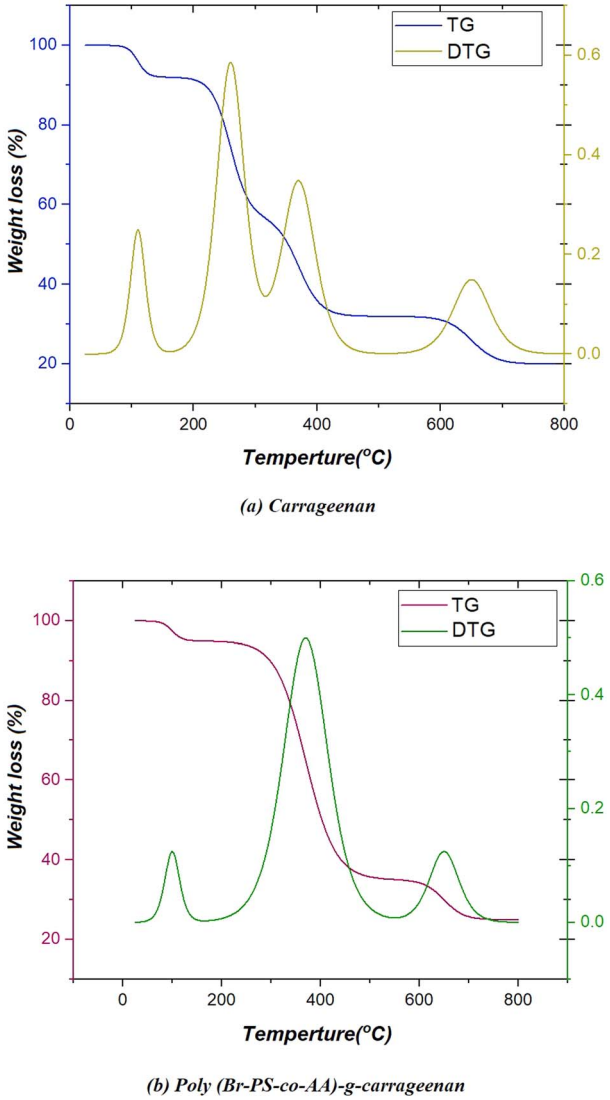

Fig. 3 TG and DTG curves of (a) native carrageenan and (b) poly(Br-PS-*co*-AA)-*g*-carrageenan.

electron affinity, likely a radical or highly delocalized system. The surface morphology of proposed structure 1 showed a high η (0.626 eV) and σ (1.596 eV^{-1}) with a hard surface and less polarizable, while the proposed structure 2 had low (0.048 eV) and very high σ (20.942 eV^{-1}) with a softer surface and a highly polarizable surface, which is easier for electron distortion. The dipole moment (μ) of them is approximately 13 debye with high polarity; the electrophilicity index (ω) of structure 1 has a very high ω (42.854 eV) with a strong electrophile, and structure 1 is near zero with 0.005 eV (minimal electrophilic character). There is a variety of Max Electron Transfer (ΔN_{max}), with structure 1

Table 2 Thermal events for both native carrageenan and poly(Br-PS-*co*-AA)-*g*-carrageenan, including the onset temperature (T_{onset}), temperature of 50% weight loss (T_{50}), and final residue percentage

Sample	T_{onset} (°C)	T_{50} (°C)	Residue at 800 °C (%)
Native carrageenan	~200 °C	~310 °C	~20%
Poly(Br-PS-*co*-AA)-*g*-carrageenan	~280 °C	~420 °C	~25%

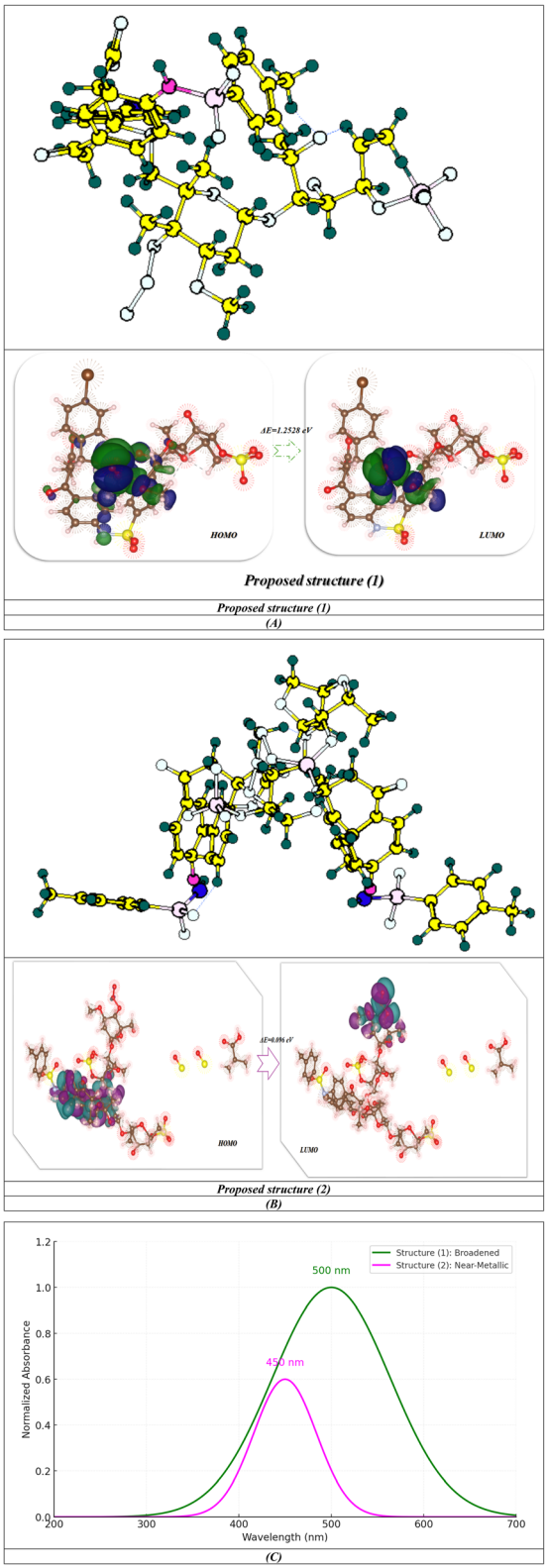

Fig. 4 (A–C) Optimized structures, HOMO–LUMO gap energy, and TD-DFT structures for the poly(Br-PS-*co*-AA)-*g*-carrageenan utilized DFT/B3LYP/6-31G(d) basis set.

Table 3 Physical descriptors for the proposed structures of poly(Br-PS-*co*-AA)-*g*-carrageenan, employing the DFT/B3LYP/6-31G(d) basis set

	Proposed structure (1)	Proposed structure (2)
E_T (au)	−2398.23	−3984.09
E_{HOMO} (eV)	−7.9536	−0.0691
E_{LUMO} (eV)	−6.7008	0.0264
E_g (eV)	1.252822	0.096
μ (D)	13.2691	12.981
χ (eV)	7.327	0.021
η (eV)	0.626	0.048
σ (eV)	1.596	20.942
P_i (eV)	−7.327	−0.021
S (eV)	0.798	10.471
Ω (eV)	42.854	0.005
ΔN_{max}	11.704472	0.4375

having a high ΔN_{max} (11.704), which can accept many electrons in a reaction, and structure 2 having a low ΔN_{max} (0.4375), which limits electron acceptance. Therefore, we concluded that structure 1 is a hard, polar, and electrophilic molecule with moderate reactivity, while structure 2 is a soft, near metallic, highly polarized system with extreme reactivity, and possibility for conductivity. The TD-DFT of these two proposed structures showed different wavelengths. Structure 1 showed a single broad absorbance at 500 nm and exhibited a HOMO–LUMO energy gap of ∼2.48 eV. The TD-DFT of structure 2 with a sharper peak at 450 nm (∼2.75 eV) is a characteristic of a radical-specific electronic transition and is a slightly larger transition energy for that excitation, even though the material overall behaves more like a near-metal. Additionally, structure 1 showed an FWHM of ∼150 nm with a wide full-width at half-maximum, indicating considerable vibronic coupling or a distribution of closely spaced excited states. In practice, this often means that the molecule has multiple conformations or extended conjugation that smears out its absorption, while structure 2, which shows an FWHM of ∼80 nm, has a tighter absorption peak, implying a more discrete electronic transition, as shown in Fig. 4(C).

We concluded that theoretical calculations were performed using two representative fragments of the synthesized copolymer: one with one carrageenan unit (structure 1) and another with two repeating units (structure 2) that were covalently bonded to Br-PS and acrylic acid. These truncated models were selected because the computational cost for a full polymer chain would be prohibitive at the DFT/B3LYP/6-31G(d) level, while short segments still preserve the essential electronic interactions (hydroxyl, sulfonamide, and carbonyl groups) that contribute to reactivity and binding. This approach is consistent with previous DFT studies on polysaccharide-based graft copolymers and provides reliable descriptors of the electronic hardness, charge transfer, and dipole moments relevant to the observed cytotoxicity from the experiments. To focus on the findings, the DFT results were compiled to show relationships with the SEM, FT-IR, and biologically relevant data. Structural 2 was more reactive and had a much lower HOMO–LUMO gap (0.096 eV), suggesting the reason for the better grafting efficiency and stronger binding in docking/MTT assays, while structural 1 had a much larger gap (1.25 eV), indicating that it is less reactive and has a more rigid configuration like that of carrageenan. The electrophilicity index (in volts, eV) calculated for structure 1 ($\omega = 42.85$ eV) is very high, whereas for structure 2 ($\sigma = 20.94$ eV^{-1}) it shows a significantly higher electronic softness than structure 1. Therefore, both these characteristics indicate a higher propensity for both structures to donate and accept electrons, giving rise to a stronger attraction to the active sites that were identified through docking analysis. Furthermore, these electronic properties support the experimental results regarding the upregulation and downregulation of gene expression. Finally, both structures have quite similar dipole moments (approximately 13 D each), suggesting that they possess segments of very strong charge polarity along the polymer chain, which is typical of sulfonated polysaccharide moieties. The discussion surrounding the HOMO–LUMO gaps now describes them only as qualitative evidence of relative reactivity and charge-transfer potential within the grafted functional groups and not as absolute band gaps for bulk polymeric materials. Representative oligomeric segments (one and two repeating units of carrageenan) were subjected to DFT optimization to model the electronic and structural characteristics of the graft copolymer. The optimized geometries indicate strong electronic coupling between the carrageenan backbone and Br-PS/acrylic acid segments. The experimental grafting degree (66.5%) and results from EDX elemental analysis quantitatively support the proposed composition, and DFT-theoretically derived energy gap and dipole moment indicate that the grafted network is more reactive and stable.

4. Biological activity investigation

4.1. Assessment of *in vitro* cytotoxic efficacy

Using the neutral red uptake test, which is based on viable cell ability to incorporate and bind the supravital dye neutral red in the lysosomes, the impact of the synthetic compounds, carrageenan and poly(Br-PS-*co*-AA)-*g*-carrageenan, on cell growth was assessed on the studied cell lines, comprising A549 and MDCK cells, with varying concentrations (25, 50, 100, and 200 μg/mL). The reference drug doxorubicin (Dox) exhibited an IC_{50} value of 16.1 μg/mL against A549 cells. After 48 hours of treatment, the viability of the A549 and MDCK cells was not significantly impacted using DMSO as a solvent. The data shown in Table 4 demonstrate that, compared to the control values, the compounds investigated had a significant impact on the A549 and MDCK cells. According to the results shown in Table 4 and Fig. 5(A), the compounds upon treatment had inhibited action against A549 cancer cells in the following order: compound poly(Br-PS-*co*-AA)-*g*-carrageenan > carrageenan. In comparison to Dox, poly(Br-PS-*co*-AA)-*g*-carrageenan (12.3 μg/mL) exhibited higher inhibitory effects after 48 hours. In addition, carrageenan demonstrated moderate suppression of A549 cancer cell proliferation when compared to the control values. Each compound's selectivity index (SI), which indicated its overall activity, was determined utilizing the IC_{50} values for

Table 4 Cytotoxic impact of the investigated compounds on A549 cells, shown as IC_{50} (μg/mL) ± SEM

	IC_{50}[a] (μg/mL) ± SEM		(SI)[b]
Compounds	A549	MDCK	A549
Doxorubicin	16.1 ± 0.02*	147.1 ± 0.05*	9.1
Carrageenan	34.3 ± 0.06*	79.2 ± 0.02*	2.3
Poly(Br-PS-*co*-AA)-*g*-carrageenan	12.3 ± 0.04*	144.4 ± 0.06*	11.7

[a] IC_{50} is the concentration required to cause a 50% reduction in cell viability. [b] (SI) = IC_{50} MDCK cell/IC_{50} A549 cell. * significant difference from control values at $p > 0.05$.

doxorubicin and the tested compounds on A549 and MDCK cells, respectively. By comparing each compound's cytotoxic activity (IC_{50}) against the cancer A549 cells with that of the normal MDCK cells, the selectivity of the cytotoxic impact of the examined compounds was observed. All the tested compounds showed significant SI values: 9.1, 11.7, and 2.3 for Dox, poly(Br-PS-*co*-AA)-*g*-carrageenan, and carrageenan on A549 cells, respectively (Table 4 and Fig. 5(A and B)). The presented findings illustrating that poly(Br-PS-*co*-AA)-*g*-carrageenan exerted the most significant and selective cytotoxic impact on A549 lung cancer cells.

4.2. Structure–activity relationship

In accordance with the structural activity relationship investigation, the cytotoxic activity of these compounds was impacted by the coupling of the carrageenan moiety with Br-PS. After 48 hours of incubation, the Br-PS moiety was added to carrageenan to yield poly(Br-PS-*co*-AA)-*g*-carrageenan, which was more effective than the original carrageenan compound against A549 cells. These findings point out the importance of the Br-PS ring as an anticancer pharmacophore.

4.3. *Molecular docking analysis of the developed anticancer agent*

Carrageenan, poly(Br-PS-*co*-AA)-*g*-carrageenan, and doxorubicin were molecularly docked using the MOE program[40,41] with the epidermal growth factor receptor tyrosine kinase domain and the 4-anilinoquinazoline inhibitor erlotinib (PDBID: 1M17)[43] for the A549 tumor cells, as illustrated in Fig. 6 and Table 5. The interaction with PDBID: 1M17 showed binding affinity of poly(Br-PS-*co*-AA)-*g*-carrageenan (−16.84 kcal mol^{-1}), followed by carrageenan (−15.83) and doxorubicin (−14.93) due to more interaction between them, and their inhibitory constant (K_i) showed high potency with poly(Br-PS-*co*-AA)-*g*-carrageenan (7.983 nM) is slightly more potent than carrageenan (8.98 nM) and doxorubicin (10.83 nM) and their binding interaction showed carrageenan and poly(Br-PS-*co*-AA)-*g*-carrageenan share interactions with Tyr 740 and Lys 836 which showed strong electrostatic interaction with amino acids (Lys/Asp/Glu), π-cation (Tyr 740), while carrageenan showed H-bonds (Arg 807, Glu 673), hydrophobic (Leu 837, Ala 674), while doxorubicin binds to different residues H-bonds (Gln 677, Asn 676), π-stacking (Tyr 803). The van der Waals, H-bonds, and desolvation energies for poly(Br-PS-*co*-AA)-*g*-carrageenan with a value of −15.83 kcal mol^{-1} and more ionic interaction. RMSD value of the grafted carrageenan showed 0.73 Å, indicating the best stable position inside the pocket of protein. The MD trajectories showed the RMSD with stable binding [poly(Br-PS-*co*-AA)-*g*-carrageenan > carrageenan > doxorubicin], and their Heatmap: reveals key residues driving interactions (electrostatic *vs.* hydrophobic), and poly(Br-PS-*co*-AA)-carrageenan is most stable with RMSD (∼0.7–1.5 Å), and its heat map showed binds charged residues (Lys730/Asp737) >90% of simulation time.

4.4. Gene expression outcomes

Using the values of IC_{50} for the examined compounds [carrageenan and poly(Br-PS-*co*-AA)-*g*-carrageenan] after 48 hours, the impact of these compounds on the mRNA expression levels of the C-myc, P21, and Cyclin D1 genes was assessed. This was achieved by calculating the ratio of their expression to that of β-Actin and comparing it to control values. C-myc and Cyclin D1 expression levels are known to be upregulated in A549 cells, while P21 gene levels are downregulated in A549 cells according to previous studies.[68–71] Current results show that doxorubicin significantly increased the expression levels of the P21 gene (∼970%) while significantly decreasing gene levels of the C-myc and Cyclin D1 genes (∼50% and 43%) relative to control values in A549 cells ($p < 0.05$) (Fig. 7). Similarly, compared to control values, poly(Br-PS-*co*-AA)-*g*-carrageenan significantly increased the expression levels of P21 genes (∼850%) while significantly decreasing levels of C-myc and Cyclin D1 (∼60% and 77%) in A549 cells ($p < 0.05$) (Fig. 7). Meanwhile, carrageenan significantly increased the P21 gene only (∼270%) in A549 cells compared to control values ($p < 0.05$) (Fig. 7). These results indicate that poly(Br-PS-*co*-AA)-*g*-carrageenan inhibits cell growth by downregulating C-myc and Cyclin D1, two important genes that promote cell cycle progression and proliferation. Concurrently, this compound increases P21, a tumor suppressor and cell cycle inhibitor that stops cells from going through the cell cycle and initiates apoptotic signaling pathways. Together, these molecular changes prevent uncontrolled cell division, inhibit the growth of tumor cells, and encourage programmed cell death, which explains the anticancer efficacy against A549 cells.

Chemotherapy is an essential part of lung cancer treatment. The majority of chemotherapeutic drugs induce apoptosis by causing DNA damage or interfering with DNA replication.[72] Since they may be possible targets for cancer treatment, the myc proto-oncogenes—genes encoding transcription factors—have been thoroughly studied. These genes are frequently overexpressed in cancer patients. In several human malignancies, myc is linked to both carcinogenesis and tumor maintenance. L-myc, N-myc, and C-myc are essentially the proteins that make up the myc family.[73–75] C-myc demonstrates a wide range of critical roles, considering the control of signaling in both healthy and malignant cells. Angiogenesis, genomic stability, cell proliferation, division, differentiation, and cell survival and death are all impacted by C-myc.[76] C-myc inhibits P21 expression by binding to the P21 promoter.[77] Xiao *et al.* demonstrated that C-

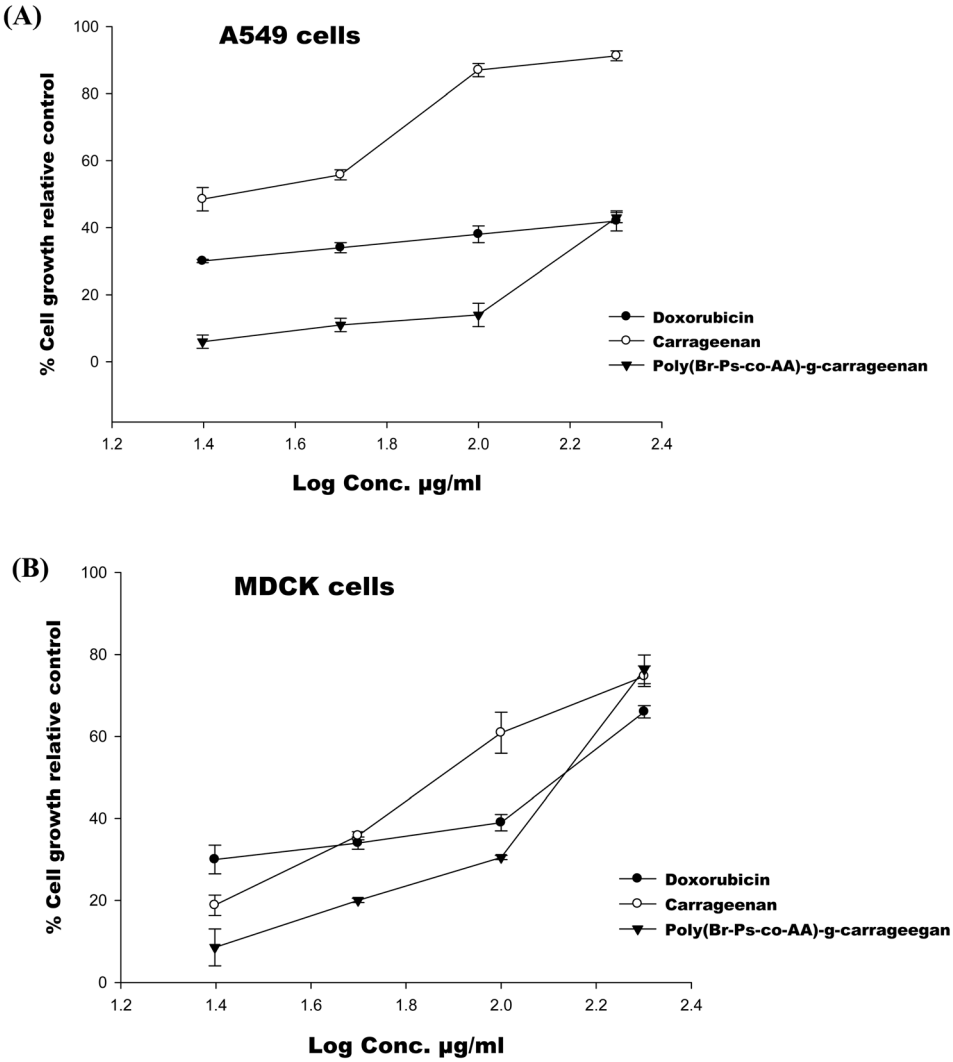

Fig. 5 (A and B) Effects of carrageenan and poly(Br-PS-*co*-AA)-*g*-carrageenan on A549 and MDCK cells after 48 hours.

myc is upregulated and P21 is downregulated when liver receptor homolog-1 (LRH-1) is expressed ectopically, which is elevated in HCC. Tumor development and cell proliferation were reduced when LRH-1 was knocked off.[78] One of the most important mechanisms for regulating the growth of cancer cells is the cell cycle in carcinogenesis. It is controlled by the synchronized activation of the cyclin-dependent kinase (CDK)/cyclin complex. In particular, the phosphorylation of tumor suppressor proteins can regulate the activation of the cyclin E/CDK2 complex at the early phase (G1/S) of the cell cycle when Cyclin E contacts CDK2.[79,80] Cyclin kinase inhibitors P21 and P27 bind to CDK and proliferating cell nuclear antigen (PCNA) to control CDK. After that, P21 and P27 cause cancer cell cycle arrest and stop DNA synthesis, which prevents the growth of cancer cells.[81] Previous studies have demonstrated the anti-apoptotic function of cytoplasmic P21 in senescent breast cancer cells induced by CDK4/6 inhibitors.[82] P21 has an environmentally dependent function in apoptosis and binds to and inhibits cyclin/CDK activity, causing cell cycle growth arrest.[83] Cyclins drive cells through the cell cycle by coordinating with their cyclin-dependent kinases.[15] Among these, the well-known cell cycle regulator Cyclin D1 (CCND1) combines with CDK4/6 to generate a complex that encourages Rb phosphorylation and deactivation so that it can move from the G1 to S phase. Nevertheless, Cyclin D1 overexpression and accumulation may act as an oncogenic protein in a number of cancer cells and cause genetic alterations in other cell cycle regulating proteins.[84,85]

4.5. Docking investigation and MD of genes

The crystal structure docking of MS0802, the c-Myc-1 binding protein domain from *Homo sapiens* (PDBID: 2yy0)[45] and the structure of the 16S rRNA methylase RmtB, P21(PDBID: 3RFH),[46] revealed interesting findings, as presented in Fig. 8 and Table 6. First, PDBID: 2yy0 showed that poly(Br-PS-*co*-AA)-*g*-carrageenan has the strongest binding affinity (BE = -13.96 kcal mol^{-1}, K_i = 8.92 µM), making it the most potent inhibitor. Carrageenan (BE = -10.86 kcal mol^{-1}, K_i = 10.83 µM) and doxorubicin (BE = -9.54 kcal mol^{-1}, K_i = 11.01 µM) showed weaker but comparable binding abilities. The

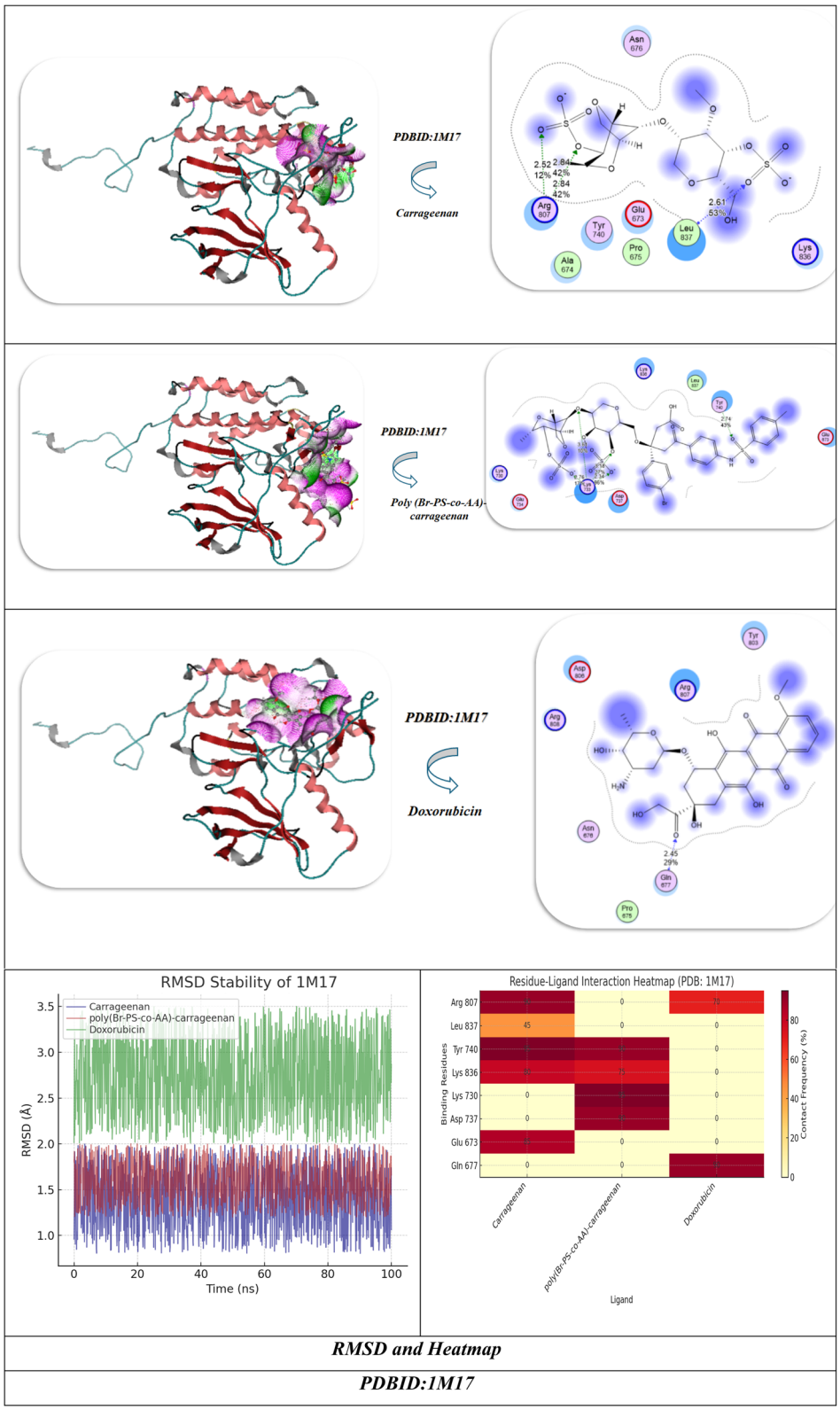

Fig. 6 Molecular docking analysis, molecular dynamic stimulation of carrageenan, poly(Br-PS-*co*-AA)-*g*-carrageenan, and doxorubicin with PDBID: 1M17.

Table 5 Energetics of all conformers of proteins with carrageenan, poly(Br-PS-*co*-AA)-*g*-carrageenan, and doxorubicin with different torsion angles

PDBID: 1M17

Compounds	Binding energy (BE)	Binding distance	Inhibitory constant, K_i (μM)	Binding amino acids	vdW + H bond + desolv energy	Electrostatic energy	Total internal, unbound energy	RMSD
Carrageenan	−15.83	2.52, 2.84, 2.61	8.98 nM	Arg 807, Leu 837, Glu 673, Tyr 740, Ala 674, Lys 836	−45.98	−12.83	−43.92	0.82
Poly(Br-PS-*co*-AA)-carrageenan	−16.84	2.34, 2.76, 3.62, 2.74	7.983 nM	Lys 730, Lys 733, Asp 737, Glu 734, Tyr 740, Lys 836	−50.83	−15.83	−46.95	0.73
Doxorubicin	−14.93	2.45	10.83 nM	Gln 677, Pro 675, Asn 676, Arg 808, Arg 807, Tyr 803	−42.92	−11.34	−39.92	0.88

interaction of the carrageenan was bonded *via* Lys B75, Glu C58, Lys A73, and Glu A77, suggesting electrostatic/ionic interactions due to charged residues. Poly(Br-PS-*co*-AA)-*g*-carrageenan interacted with 6 residues (ProA57, Glu B61, Asn C59, Glu C63, Glu C58, and Arg C66), including both polar and charged residues divided into electrostatic: Glu B61, Glu C58, and Glu C63 (negative) + Arg C66 (positive); H-bonding: Asn C59 (polar); and hydrophobic: ProA57. The presence of Br might enhance van der Waals interactions *via* halogen bonding with aromatic/proline residues. Carrageenan is a linear polysaccharide that showed sulfate groups likely forming salt bridges with Lys A73/B75 and Glu A77/C58. Doxorubicin binds fewer residues (Lys A73, Glu B68, and Glu 58) and may stack against hydrophobic pockets (*e.g.*, near ProA57), showing weak electrostatic energy despite binding Glu/Lys; it lacks the multi-residue engagement observed in carrageenans, possibly relying more on hydrophobic/aromatic stacking. The van der Waals, H-bond, and desolvation of poly(Br-PS-*co*-AA)-*g*-carrageenan had the strongest contribution (−28.49 kcal mol^{-1}), indicating robust hydrophobic packing/H-bonding, carrageenan (−22.98 kcal mol^{-1}), and doxorubicin

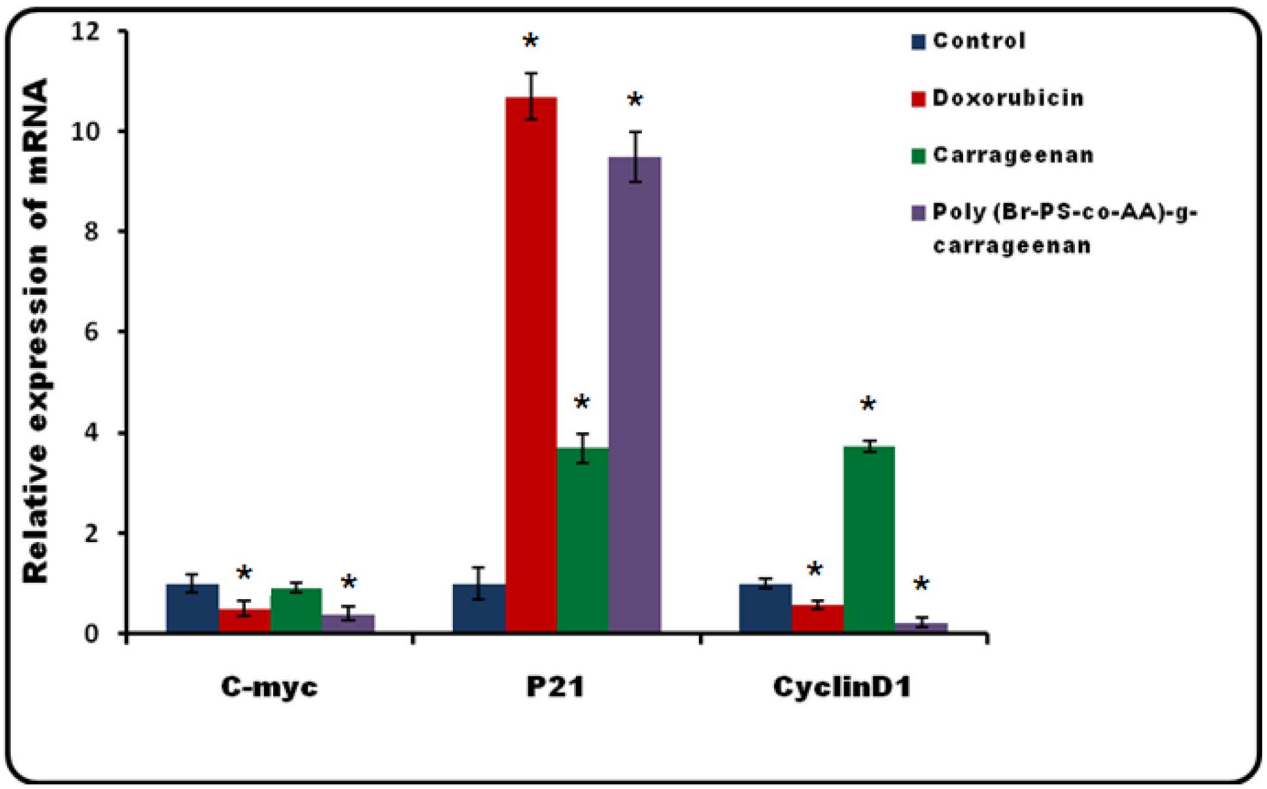

Fig. 7 Influences of doxorubicin, carrageenan, and poly(Br-PS-*co*-AA)-*g*-carrageenan on the expression levels of C-myc, P21, and Cyclin D1 mRNA in A549 cells. The data were repeatable, *, $p < 0.05$, and are shown as mean ± SEM.

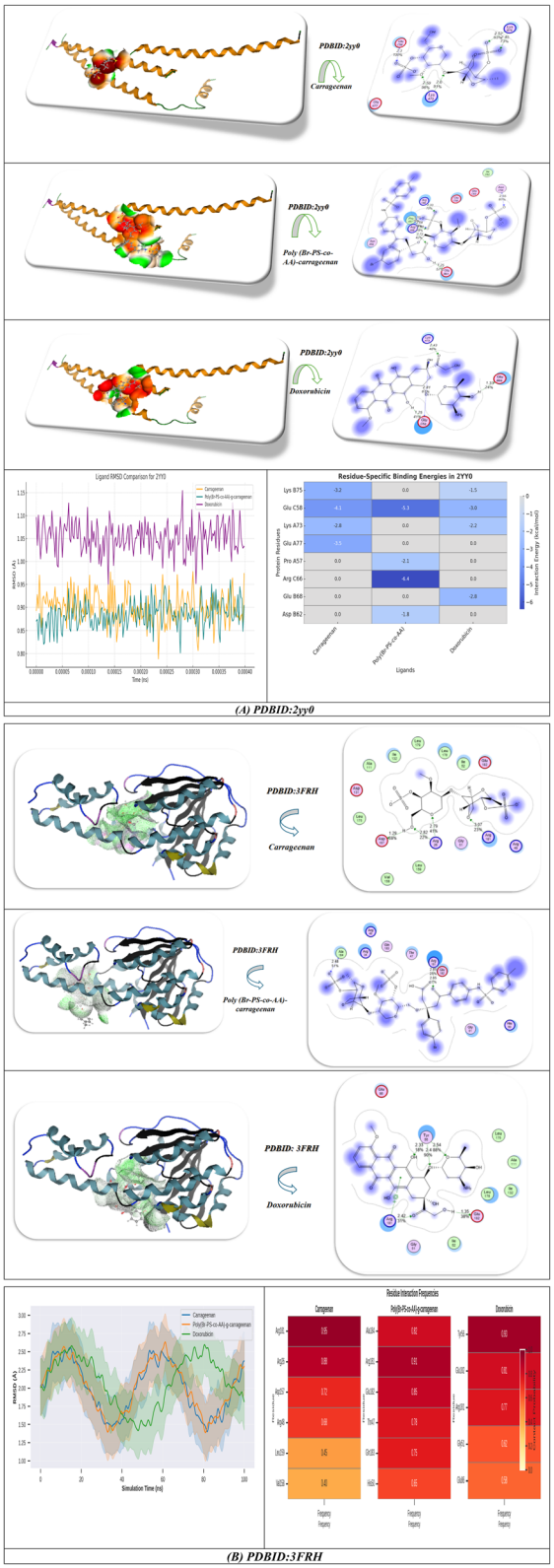

Fig. 8 (A and B) Docking and MD of carrageenan, poly(Br-PS-*co*-AA)-*g*-carrageenan, and doxorubicin with PDBID: 2yy0 and PDBID: 3FRH, respectively.

(−20.93 kcal mol^{-1}). Their RMSD showed value (0.87–0.99 Å) which suggests stable docking poses and minimal deviation, and their RMSD dynamic trajectory showed 0.90 Å, with fluctuations generally in the range of ∼0.85–0.97 Å. The fluctuations observed in carrageenan were small compared to other compounds, indicating that the carrageenan had been successfully positioned in the binding pocket (*i.e.*, the active site of the enzyme) with little deviation over a prolonged period of time. On the other hand, poly(Br-PS-*co*-AA)-*g*-carrageenan exhibited an average RMSD of approximately 0.88 Å with a narrow range of fluctuation between 0.82 and 0.94 Å. This lower average and tighter stability range than native carrageenan suggests that the graft copolymer had a greater degree of constraint on ligand motion within the binding pocket compared to the native ligand. Doxorubicin, however, displayed the highest average RMSD (roughly 1.02 Å), with a wider range of fluctuation (about 1.00 to 1.15 Å) compared to the other two ligands; this higher value suggests that doxorubicin was more mobile within the active site and had undergone greater conformational changes during the course of simulation. The heat map of poly(Br-PS-*co*-AA)-*g*-carrageenan shows the deepest blue at Arg C66 (−6.4 kcal mol^{-1}) and strong contact with Glu C58 (−5.3 kcal mol^{-1}), indicating tight binding *via* those residues. Carrageenan had its strongest contacts with Glu C58 (−4.1 kcal mol^{-1}) and Glu A77 (−3.5 kcal mol^{-1}), indicating electrostatic anchoring to those glutamates, and doxorubicin interacted most favorably with Lys B75 (−1.5 kcal mol^{-1}) and Glu B68 (−2.8 kcal mol^{-1}) but overall showed weaker binding energies compared to the polysaccharide ligands.

The perceived differences in the strength of interaction when binding PDBID:3RFH with carrageenan, poly(Br-PS-*co*-AA)-*g*-carrageenan & doxorubicin have been documented. The interaction of PDBID:3RFH with poly(Br-PS-*co*-AA)-*g*-carrageenan had the strongest binding affinity (−9.64 kcal mol^{-1}), followed by carrageenan (−8.05 kcal mol^{-1}) and lastly, doxorubicin (−7.05 kcal mol^{-1}). These values are consistent with the inhibition constants at which these compounds are effective at inhibiting the protein (K_i). The inhibition constant for poly(Br-PS-*co*-AA)-*g*-carrageenan ($K_i = 9.08$ μM) is the lowest of the three and therefore represents the most potent inhibitor, while both carrageenan and doxorubicin had comparable K_i values (∼10.75–10.81 μM), indicating their relatively lower potential to inhibit compared to poly(Br-PS-*co*-AA)-*g*-carrageenan. Moreover, the binding distance of all compounds is ≤3.07 Å, indicating strong interactions, such as hydrogen bonds and ionic interactions. Doxorubicin has the shortest interaction (1.35 Å), likely with a charged residue (*e.g.*, Glu 86 or Arg 181). The interaction with amino acids showed that carrageenan interacts with positively charged residues (Arg 26, Arg 48, Arg 181) and hydrophobic residues (Leu 159, Val 158), suggesting electrostatic and van der Waals forces with ionic (+charge attraction to sulfate); poly(Br-PS-*co*-AA)-*g*-carrageenan binds to a mix of polar (Gln 183, His 50) and charged (Glu 182) residues, indicating diverse interactions due to the electron-withdrawing effect with the Br atom and hydrogen bonding. Doxorubicin targets Tyr 56 (aromatic) and Glu 86 (negative charge), hinting at π-stacking and salt bridges. Their energy contribution showed that electrostatic energy is significant for carrageenan (−9.8 kcal mol^{-1}),

Table 6 Energetics of all conformers of proteins with carrageenan, poly(Br-PS-*co*-AA)-*g*-carrageenan, and doxorubicin with PDBID: 2yy0 and PDBID: 3FRH

Compounds	Binding energy (BE)	Binding distance	Inhibitory constant, K_i (μM)	Binding amino acids	vdW + H bond + desolv energy	Electrostatic energy	Total internal, unbound energy	RMSD
PDBID: 2yy0								
Carrageenan	**−10.86**	2.52, 2.3, 2.6, 2.59	10.83	Lys B75, Glu C58, Lys A73, Glu A77	−22.98	−10.83	−18.83	0.92
Poly(Br-PS-*co*-AA)-carrageenan	**−13.96**	3.03, 2.72, 1.25, 2.55	8.92	ProA57, Glu B61, Asn C59, Glu C63, Glu C58, Arg C66	−28.49	−14.30	−23.84	0.87
Doxorubicin	**−9.54**	1.25, 2.81, 1.33, 2.43	11.01	Lys A73, Glu B68, Glu 58	−20.93	−9.93	−14.75	0.99
PDBID: 3FRH								
Carrageenan	−8.05	1.29, 2.82, 2.79, 3.07	10.75	Arg 181, Arg 26, Asp 157, Arg 48, Leu 159, Val 158	−27.95	−9.8	−31.50	0.99
Poly(Br-PS-*co*-AA)-carrageenan	−9.64	2.85, 2.65, 2.48	9.08	Ala 184, Arg 181, Glu 182, Thr 47, Gln 183, His 50, Gly 51	−30.30	−10.36	−33.92	0.93
Doxorubicin	−7.05	2.54, 2.33, 2.42, 1.35	10.81	Tyr 56, Glu 182, Arg 181, Gly 51, Glu 86	−26.96	−8.65	−28.52	1.02

aligning with its Arg-rich binding site. Poly(Br-PS-*co*-AA)-*g*-carrageenan (−33.92 kcal mol^{-1}) reflects high stability for all internal energy. The RMSD of poly(Br-PS-*co*-AA)-*g*-carrageenan has the lowest RMSD (0.93 Å), suggesting an optimal fit. The dynamic stimulation of RMSD with time in ns showed that poly(Br-PS-*co*-AA)-*g*-carrageenan (orange) dips to the lowest minimum (∼1.0 Å at ∼40 ns), suggesting that it holds the protein backbone most tightly in that middle window. Its fluctuations (shaded band) also narrow most here, pointing to increased rigidity. Native carrageenan (blue) is intermediate; its minimum (∼1.3 Å) and fluctuation bandwidth sit between the polymer and doxorubicin, indicating moderate stabilization. Doxorubicin (green) showed the highest peaks (∼3.0 Å) and the overall widest shaded band, reflecting the greatest backbone drift and flexibility throughout the run. Their heat map showed carrageenan with Arg181 (0.95) and Arg26 (0.88) are the hottest spots; these two arginines form salt bridges or strong electrostatic contacts nearly the entire time, and Asp157 (0.72) and Arg48 (0.68) are also moderately engaged likely through a mix of charge and hydrogen bonding. Leu159 (0.45) and Val158 (0.40) showed weaker, more transient hydrophobic packing. In addition, poly(Br-PS-*co*-AA)-*g*-carrageenan demonstrates its highest interactions with arginine at position 181 and glutamic acid at position 182, which were previously observed; however, now, additional interactions become significantly stronger such as alanine at position 184, threonine at position 47, glutamine at position 183, and histidine at position 50 forming the complete top set of poly(Br-PS-*co*-AA)-*g*-carrageenan to PERIPHERALLY locate ligands compared to carrageenans. The presence of other grafted chains provides additional ionic contacts (*i.e.*, charged and polar), enabling poly(Br-PS-*co*-AA)-*g*-carrageenan to increase contact with the binding pocket over carrageenan. Doxorubicin interacts with Tyr56 (0.93) as the standout, reflecting persistent π–π stacking or hydrogen bonding with the aromatic core of doxorubicin. The residues Glu182 (0.81) and Arg181 (0.77) were also included in the interaction, but their influence was weaker than that of the polysaccharide complexes. Gly51 (0.62) and Glu86 (0.58) provided secondary contributions to the overall major contacts. In summary, Tyr56, as the only aromatic hotspot for ligand attachment and with relatively few electrostatic stabilizing points, produced a more confined and localized binding footprint than carbohydrate-based ligands.

The data for quantitative binding are presented in Tables 4 and 5. Against EGFR (1M17), poly(Br-PS-*co*-AA)-*g*-carrageenan has the best binding energy (−16.84 kcal mol^{-1}) from hydrogen bonding to Lys 730, Asp 737, and Tyr 740, surpassing carrageenan (−15.83) and doxorubicin (−14.93). For C-myc (2yy0), binding energy was ranked poly(Br-PS-*co*-AA)-*g*-carrageenan (−13.96) > carrageenan (−10.86) > doxorubicin (−9.54). The grafted polymer achieved a binding energy of −9.64 kcal mol^{-1} against P21 (3RFH) with stable hydrogen bonding to Arg 181, Glu 182, and Gln 183. The corresponding inhibitory constants (K_i) were 7.98 nM (EGFR) to 9.08 μM (P21), demonstrating strong and selective binding. After validating the dynamic aspects of the receptors *via* molecular dynamics (MD) at 50 ns in the GROMACS MD program using AMBER/CHARMM force field at 300 K with explicit solvation, the resulting RMSD values of approximately 0.7–1.0 Å indicated that the complexes had reached equilibrium. The heat map analyses also showed continuous presence of electrostatic and hydrogen bond interactions throughout the trajectories which corresponded with the observed activity in experiments. Example ligand-receptor binding mode diagrams are shown in Fig. 6 and 8.

4.5.1. Docking mechanism. To provide additional clarity concerning the link between the *in silico* and *in vitro* outcomes of this research, we included an explanatory paragraph describing the mechanistic link between the docking results

and our observed biological responses. The molecular docking and MD simulations now provide a direct context for the experimental results by demonstrating how poly(Br-PS-*co*-AA)-*g*-carrageenan interacts with important molecular targets to produce the observed cellular effects in A549 lung cancer cells. The strong binding energy with EGFR (-16.84 kcal mol^{-1}) indicates inhibition of EGFR-mediated phosphorylation cascades that reduce cyclin D1 and halt unregulated proliferation. The strong binding affinity observed for C-myc (-13.96 kcal mol^{-1}) due to important amino acids (or residues), such as Lys A73, Glu C58, and Arg C66, suggests that the C-myc/Max transcriptional complex may be disrupted. This is consistent with the fact that C-myc has been experimentally shown to regulate the oncogenic C-myc pathway downwards. Additionally, the good interaction with P21 (-9.64 kcal mol^{-1}), especially from the contact made with amino acids (Arg181, Glu182, and Gln183), indicate that P21 could also be activated. This supports its known function of inducing G1 cell cycle arrest and apoptosis. All these molecular events represent a mechanistic pathway that can be summarized as follows: docking → receptor inhibition (EGFR, C-myc) → signaling suppression → P21 activation → cell-cycle arrest → apoptosis. This causal chain crosses the computational predictions and the biological outcome formed by the polymer's strong and stable target engagement, leading to observable transcriptional modulation and cytotoxicity. Dynamic simulations (RMSD ≈ 0.7–1.0 Å) validated the conformational stability of each complex for 50 ns, which indicates continuous binding on the same time scale as the experimental incubation (48 h). The achieved rigidity and stable hydrogen-bond occupancy had corresponding antiproliferative activity observed in the lab. The docking and MD analyses corroborate the experimental gene-expression data, indicating that poly(Br-PS-*co*-AA)-*g*-carrageenan tightly binds to EGFR and C-myc, decreasing their transcriptional activity while stabilizing P21, and resulting in increased protein levels. This interplay between molecular binding and transcriptional response offers a cohesive mechanistic explanation for the apoptosis and growth inhibition we observed in A549 cells.

5. Conclusions

This study aimed to structure a safe, selective, effective, and low-cost anticancer agent based on carrageenan grafted with a copolymer of acrylic acid and sulfonamide derivative [poly(Br-PS-*co*-AA)-*g*-carrageenan] through free radical copolymerization. DFT and TD-DFT investigations shed light on the electronic characteristics of the synthesized grafted copolymer, indicating enhanced reactivity and molecular stability. Additionally, the structural features and surface morphology confirmed successful grafting. Poly(Br-PS-*co*-AA)-*g*-carrageenan demonstrated significant cytotoxicity activity against A549 lung cancer cells, displaying high selectivity compared to normal cells and outperforming the standard chemotherapeutic agent doxorubicin. It inhibited cell cycle progression and triggered apoptosis by upregulating the P21 gene and downregulating the Cyclin D1 and C-myc genes. Molecular docking and dynamic simulations supported these experimental findings, demonstrating strong and stable binding to crucial cancer-related sites. In conclusion, poly(Br-PS-*co*-AA)-*g*-carrageenan represents a safe, promising, and successful therapeutic approach for targeted lung cancer that warrants further *in vivo* research and preclinical development.

Ethical approval

The Medical Research Ethics Committee, National Research Center, Dokki, Giza, Egypt, gave its approval to this research (approval number 11431223).

Conflicts of interest

There are no conflicts to declare.

Data availability

The data supporting this study's findings are available from the corresponding author, M. S. Hashem, on request.

Acknowledgements

The study, writing and publication of this work were done without any financial assistance for the authors.

References

1 Z. Yang, H. Yang and H. Yang, Effects of sucrose addition on the rheology and microstructure of κ-carrageenan gel, *Food Hydrocolloids*, 2018, **75**, 164–173.
2 S. Toumi, *et al.*, Synthesis, characterization and potential application of hydrophobically modified carrageenan derivatives as pharmaceutical excipients, *Carbohydr. Polym.*, 2021, **251**, 116997.
3 F. Shabani, R. Karimi-Soflou and A. Karkhaneh, Folate-mediated targeting of carrageenan-cholesterol micelles for enhanced breast cancer treatment, *Eur. Polym. J.*, 2024, **208**, 112852.
4 L. Youssouf, *et al.*, Enhanced effects of curcumin encapsulated in polycaprolactone-grafted oligocarrageenan nanomicelles, a novel nanoparticle drug delivery system, *Carbohydr. Polym.*, 2019, **217**, 35–45.
5 Y. Cao, *et al.*, Specific binding of trivalent metal ions to λ-carrageenan, *Int. J. Biol. Macromol.*, 2018, **109**, 350–356.
6 R. M. Obaidat, M. Alnaief and H. Mashaqbeh, Investigation of Carrageenan Aerogel Microparticles as a Potential Drug Carrier, *AAPS PharmSciTech*, 2018, **19**(5), 2226–2236.
7 I. Ijaz, *et al.*, Functionalization of MXene using iota-carrageenan, maleic anhydride, and N,N′-methylene bis-acrylamide for high-performance removal of thorium (IV), uranium (IV), sulfamethoxazole, and levofloxacin, *Int. J. Biol. Macromol.*, 2024, **279**, 134913.
8 M. S. Elfaruk and S. Janaswamy, Preparation and characterization of iota carrageenan-cyclodextrin-curcumin fibers and the release nature of curcumin in simulated digestion conditions, *Food Hydrocolloids*, 2024, **151**, 109785.

9 G. Venkatachalam, *et al.*, Immunomodulatory zymosan/ι-carrageenan/agarose hydrogel for targeting M2 to M1 macrophages (antitumoral), *RSC Adv.*, 2024, **14**(17), 11694–11705.
10 X. Chen, *et al.*, Iota carrageenan gold-silver NPs photothermal hydrogel for tumor postsurgical anti-recurrence and wound healing, *Carbohydr. Polym.*, 2022, **298**, 120123.
11 A. Taghikhani, *et al.*, Facile preparation of a pH-sensitive biocompatible nanocarrier based on magnetic layered double hydroxides/Cu MOFs-chitosan crosslinked κ-carrageenan for controlled doxorubicin delivery to breast cancer cells, *Colloids Surf., B*, 2024, **243**, 114122.
12 G. R. Bardajee, Z. Hooshyar and F. Rastgo, Kappa carrageenan-g-poly (acrylic acid)/SPION nanocomposite as a novel stimuli-sensitive drug delivery system, *Colloid Polym. Sci.*, 2013, **291**(12), 2791–2803.
13 N. A. Hussain and L. S. Jasim, Synthesis and characterization of kappa (κ)-carrageenan-grafted poly (acrylic acid-co-itaconic acid)/multi-walled carbon nanotube (κC-g-poly (AAC-co-IA)/MWCNT) composite for removing safranin-o dye from aqueous solution, *Process Saf. Environ. Prot.*, 2025, **195**, 106828.
14 N. Kochkina, M. Nikitina and I. Terekhova, Native and modified β-cyclodextrins as solubility enhancers for methotrexate loaded in iota-carrageenan hydrogel, *J. Mol. Liq.*, 2025, **427**, 127407.
15 X. Wang, X. Liu, Y. Yang and D. Yang, Cyclin D1 mediated by the nuclear translocation of nuclear factor kappa B exerts an oncogenic role in lung cancer, *Bioengineered*, 2022, **13**(3), 6866–6879.
16 C. Wang, Y. Yang, G. Zhang, J. Li, X. Wu, X. Ma, Y. Mei, *et al.*, Long noncoding RNA EMS connects c-Myc to cell cycle control and tumorigenesis, *Proc. Natl. Acad. Sci. U. S. A.*, 2019, **116**(29), 14620–14629.
17 J. P. Morton and O. J. Sansom, MYC-y mice: From tumour initiation to therapeutic targeting of endogenous MYC, *Mol. Oncol.*, 2013, **7**, 248–258.
18 P. Zhang, L. Cao, P. Fan, Y. Mei and M. Wu, LncRNA-MIF, a c-Myc-activated long noncoding RNA, suppresses glycolysis by promoting Fbxw7-mediated c-Myc degradation, *EMBO Rep.*, 2016, **17**, 1204–1220.
19 C. Y. Lin, *et al.*, Transcriptional amplification in tumor cells with elevated c-Myc, *Cell*, 2012, **151**, 56–67.
20 P. A. Carroll, *et al.*, The MYC transcription factor network: balancing metabolism, proliferation and oncogenesis, *Front. Med.*, 2018, **12**(4), 412–425.
21 T. Deng, *et al.*, Deubiquitylation and stabilization of p21 by USP11 is critical for cell-cycle progression and DNA damage responses, *Proc. Natl. Acad. Sci. U. S. A.*, 2018, **115**(18), 4678–4683.
22 E. Zlotorynski, The dark side of p21, *Nat. Rev. Mol. Cell Biol.*, 2016, **17**(8), 461.
23 T. Fu, *et al.*, p21 promotes gemcitabine tolerance in A549 cells by inhibiting DNA damage and altering the cell cycle, *Oncol. Lett.*, 2023, **26**(5), 471.
24 T. Han, *et al.*, Exploring the interaction of calycosin with cyclin D1 protein as a regulator of cell cycle progression in lung cancer cells, *Arabian J. Chem.*, 2022, **15**(5), 103722.
25 P. Ramos-García, M. Á. González-Moles, A. Ayen, L. González-Ruiz, J. A. Gil-Montoya and I. Ruiz-Ávila, Predictive value of CCND1/cyclin D1 alterations in the malignant transformation of potentially malignant head and neck disorders: Systematic review and meta-analysis, *Head Neck*, 2019, **41**(9), 3395–3407.
26 F. I. Montalto and F. De Amicis, Cyclin D1 in cancer: a molecular connection for cell cycle control, adhesion and invasion in tumor and stroma, *Cells*, 2020, **9**(12), 2648.
27 P. Ramos-Garcia, M. Á. González-Moles, L. Gonzalez-Ruiz, I. Ruiz-Avila, A. Ayen and J. A. Gil-Montoya, Prognostic and clinicopathological significance of cyclin D1 expression in oral squamous cell carcinoma: A systematic review and meta-analysis, *Oral Oncol.*, 2018, **83**, 96–106.
28 M. S. Hashem, H. S. Magar, A. M. Fahim and R. A. Sobh, Antimicrobial, antioxidant, mechanistic, docking simulation, and electrochemical studies for grafting polymerization of novel sulphonated gelatin derived from chicken feet, *Mater. Chem. Phys.*, 2023, **310**, 128474, DOI: 10.1016/j.matchemphys.2023.128474.
29 M. S. Hashem, R. A. Sobh, A. M. Fahim and G. H. Elsayed, Alginate sulfonamide hydrogel beads for 5-fluorouracil delivery: antitumor activity, cytotoxicity assessment, and theoretical investigation, *Int. J. Biol. Macromol.*, 2024, **282**(Part 1), 136573.
30 M. S. Hashem and H. S. Magar, Creative synthesis of pH-dependent nanoporous pectic acid grafted with acrylamide and acrylic acid copolymer as an ultrasensitive and selective riboflavin electrochemical sensor in real samples, *Int. J. Biol. Macromol.*, 2024, **280**(Part 4), 136022.
31 A. Frisch, *Gaussian 09W Reference*. Wallingford, USA, 25p, 2009.
32 A. M. Fahim and E. E. Abu-El Magd, Enhancement of Molecular imprinted polymer as organic fillers on bagasse cellulose fibers with biological evaluation and computational calculations, *J. Mol. Struct.*, 2021, **1241**, 130660.
33 A. M. Fahim and A. M. Farag, Synthesis, antimicrobial evaluation, molecular docking and theoretical calculations of novel pyrazolo [1, 5-a] pyrimidine derivatives, *J. Mol. Struct.*, 2020, **1199**, 127025.
34 M. S. Hashem, A. M. Fahim and F. M. Helaly, Designing a green poly (β-amino ester) for the delivery of nicotinamide drugs with biological activities and conducting a DFT investigation, *RSC Adv.*, 2024, **14**, 5499–5513.
35 N. H. Mahmoud and A. M. Fahim, The Effect of Anion, Steric Factors on the Catalytic Activity of Hydrogen Peroxide, Biological Activities, Docking, and DFT Calculations of Novel Mixed Ligand of Copper Complexes, *Appl. Organomet. Chem.*, 2025, **39**(6), e70220.
36 G. Repetto, A. Del Peso and J. L. Zurita, Neutral red uptake assay for the estimation of cell viability/cytotoxicity, *Nat. Protoc.*, 2008, **3**(7), 1125–1131.

37 P. Prayong, S. Barusrux and N. Weerapreeyakul, Cytotoxic activity screening of some indigenous Thai plants, *Fitoterapia*, 2008, **79**, 598–601.
38 K. J. Livak and T. D. Schmittgen, Analysis of relative gene expression data using real-time quantitative PCR and the 2− ΔΔCT method, *methods*, 2001, **25**(4), 402–408.
39 G. A. Elmegeed, *et al.*, Evaluation of heterocyclic steroids and curcumin derivatives as anti-breast cancer agents: Studying the effect on apoptosis in MCF-7 breast cancer cells, *Steroids*, 2016, **115**, 80–89.
40 A. M. Fahim, S. Dacrory and G. H. Elsayed, Anti-proliferative activity, molecular genetics, docking analysis, and computational calculations of uracil cellulosic aldehyde derivatives, *Sci. Rep.*, 2023, **13**(1), 14563.
41 S. Vilar, G. Cozza and S. Moro, Medicinal chemistry and the molecular operating environment (MOE): application of QSAR and molecular docking to drug discovery, *Curr. Top. Med. Chem.*, 2008, **8**(18), 1555–1572.
42 B. L. Jejurikar and S. H. Rohane, Drug designing in discovery studio, *Asian J. Res. Chem.*, 2021, **14**(2), 135–138.
43 J. Stamos, M. X. Sliwkowski and C. Eigenbrot, Structure of the Epidermal Growth Factor Receptor Kinase Domain Alone and in Complex with a 4-Anilinoquinazoline Inhibitor, *J. Biol. Chem.*, 2002, **277**(48), 46265–46272.
44 M. Yogesha, V. G. Rao, P. Devangad, J. S. D'Souza and S. A. Chidangil, A chemometric study combined with spectroscopy for the quantification of secondary structure of flagellar-associated protein 174 (FAP174), *J. Chemom.*, 2020, **34**(5), e3221.
45 E. Schmitt, *et al.*, Structural Bases for 16 S rRNA Methylation Catalyzed by ArmA and RmtB Methyltransferases, *J. Mol. Biol.*, 2009, **388**(3), 570–582.
46 A. M. Fahim, Exploring novel benzene sulfonamide derivatives: Synthesis, ADME studies, anti-proliferative activity, docking simulation, and emphasizing theoretical investigations, *J. Indian Chem. Soc.*, 2024, **101**(8), 101211.
47 D. Van Der Spoel, *et al.*, GROMACS: fast, flexible, and free, *J. Comput. Chem.*, 2005, **26**(16), 1701–1718.
48 M. S. Hashem, R. A. Sobh and M. A. Abd El-Ghaffar, pH-responsive bionanocomposite pectin grafted with dimethylaminoethyl methacrylate and acrylic acid copolymer along with silver nanoparticles for breast cancer drug delivery, *Polym. Eng. Sci.*, 2024, **64**(12), 6115–6128, DOI: 10.1002/pen.26975.
49 M. S. Hashem and H. S. Magar, Inventive pectic acid grafted with polyacrylamide for a highly sensitive and selective non-enzymatic dopamine sensor in pharmaceutical samples, *RSC Adv.*, 2025, **15**, 33758–33772.
50 M. A. Abd El-Ghaffar and M. S. Hashem, Calcium alginate beads encapsulated PMMA-g-CS nano-particles for α-chymotrypsin immobilization, *Carbohydr. Polym.*, 2013, **92**, 2095–2102.
51 M. A. Abd El-Ghaffar, M. S. Hashem, M. K. El-Awady and A. M. Rabie, pH-sensitive sodium alginate hydrogels for riboflavin controlled release, *Carbohydr. Polym.*, 2012, **89**(2), 667–675.
52 A. Portal D'Almeida, L. R. B. Gonçalves, T. Lima de Albuquerque, R. Fernandez-Lafuente and I. J. da Silva, Alcalase immobilization in iota-carrageenan-matrix hydrogel beads derived from the macroalga Solieria filiformis, *Enzyme Microb. Technol.*, 2025, **188**, 110636.
53 N. K. Farhana, F. S. Omar, R. Shanti, *et al.*, Iota-carrageenan-based polymer electrolyte: impact on ionic conductivity with incorporation of AmNTFSI ionic liquid for supercapacitor, *Ionics*, 2019, **25**, 3321–3329, DOI: 10.1007/s11581-019-02865-1.
54 L. Vandanjon, A.-S. Burlot, E. F. Zamanileha, P. Douzenel, P. H. Ravelonandro, N. Bourgougnon and G. Bedoux, The Use of FTIR Spectroscopy as a Tool for the Seasonal Variation Analysis and for the Quality Control of Polysaccharides from Seaweeds, *Mar. Drugs*, 2023, **21**, 482, DOI: 10.3390/md21090482.
55 H. S. Magar, A. M. Fahim and M. S. Hashem, Accurate, affordable, and easy electrochemical detection of ascorbic acid in fresh fruit juices and pharmaceutical samples using an electroactive gelatin sulfonamide, *RSC Adv.*, 2024, **14**, 39820–39832.
56 A. M. Fahim and M. A. Shalaby, Synthesis, biological evaluation, molecular docking and DFT calculations of novel benzenesulfonamide derivatives, *J. Mol. Struct.*, 2019, **1176**, 408–421.
57 N. A. Kheder, *et al.*, Unreported Biginelli product with potent antifungal activity: Synthesis, DFT insights, and docking simulation analysis, *J. Mol. Struct.*, 2025, **1330**, 141480.
58 H. E. M. Tolan, A. M. Fahim and E. H. I. Ismael, Synthesis, biological activities, molecular docking, theoretical calculations of some 1,3,4-oxadiazoles, 1,2,4-triazoles, and 1,2,4-triazolo[3,4-b]-1,3,4-thiadiazines derivatives, *J. Mol. Struct.*, 2023, **1283**, 135238.
59 R. G. Parr and R. G. Pearson, Absolute hardness: companion parameter to absolute electronegativity, *J. Am. Chem. Soc.*, 1983, **105**(26), 7512–7516.
60 W. Gordy and W. O. Thomas, Electronegativities of the elements, *J. Chem. Phys.*, 1956, **24**(2), 439–444.
61 P. K. Chattaraj, A. Cedillo and R. G. Parr, Chemical softness in model electronic systems: dependence on temperature and chemical potential, *Chem. Phys.*, 1996, **204**(2–3), 429–437.
62 A. Ino, *et al.*, Chemical potential shift in overdoped and underdoped La 2− x Sr x CuO 4, *Phys. Rev. Lett.*, 1997, **79**(11), 2101.
63 A. Vela and J. L. Gazquez, A relationship between the static dipole polarizability, the global softness, and the fukui function, *J. Am. Chem. Soc.*, 1990, **112**(4), 1490–1492.
64 L. R. Domingo, *et al.*, Quantitative characterization of the global electrophilicity power of common diene/dienophile pairs in Diels–Alder reactions, *Tetrahedron*, 2002, **58**(22), 4417–4423.
65 A. Hanna and M. Tinkham, Variation of the Coulomb staircase in a two-junction system by fractional electron charge, *Phys. Rev. B: Condens. Matter Mater. Phys.*, 1991, **44**(11), 5919.

66 H. E. M. Tolan, *et al.*, New mercaptopyrimidine derivatives synthesized with expected antimicrobial and antioxidant properties and theoretical study, *J. Mol. Struct.*, 2025, **1324**, 140795.
67 M. A. Shalaby, A. M. Fahim and S. A. Rizk, Microwave-assisted synthesis, antioxidant activity, docking simulation, and DFT analysis of different heterocyclic compounds, *Sci. Rep.*, 2023, **13**(1), 4999.
68 J. E. Park, J. H. Jung, H. J. Lee, D. Y. Sim, E. Im, W. Y. Park, S. H. Kim, *et al.*). Ribosomal protein L5 mediated inhibition of c-Myc is critically involved in sanggenon G induced apoptosis in non-small lung cancer cells, *Phytother. Res.*, 2021, **35**(2), 1080–1088.
69 Y. Xu, C. Wang, X. Jiang, Y. Zhang, H. Su, J. Jiang, X. Qiu, *et al.*). KLHL38 involvement in non-small cell lung cancer progression via activation of the Akt signaling pathway, *Cell Death Dis.*, 2021, **12**(6), 556.
70 S. M. M. Yahya, A. O. Abdelhamid, M. M. Abd-Elhalim, G. H. Elsayed and E. F. Eskander, The effect of newly synthesized progesterone derivatives on apoptotic and angiogenic pathway in MCF-7 breast cancer cells, *Steroids*, 2017, **126**, 15–23, DOI: 10.1016/j.steroids.2017.08.002.
71 G. H. Elsayed, A. M. Fahim and A. I. Khodair, Synthesis, anti-cancer activity, gene expression and docking stimulation of 2-thioxoimidazolidin-4-one derivatives, *J. Mol. Struct.*, 2022, **1265**, 133401.
72 L. He, L. Luo, H. Zhu, H. Yang, Y. Zhang, H. Wu, H. Sun, F. Jiang, C. S. Kathera, L. Liu, *et al*, FEN1 promotes tumor progression and confers cisplatin resistance in non-small-cell lung cancer, *Mol. Oncol.*, 2017, **11**, 640–654.
73 P. Chanvorachote, N. Sriratanasak and N. Nonpanya, C-myc contributes to malignancy of lung cancer: a potential anticancer drug target, *Anticancer Res.*, 2020, **40**(2), 609–618.
74 J. R. Whitfield, M. E. Beaulieu and L. Soucek, Strategies to inhibit Myc and their clinical applicability, *Front. Cell Dev. Biol.*, 2017, **5**, DOI: 10.3389/fcell.2017.00010.
75 J. Bragelmann, S. Bohm, M. R. Guthrie, G. Mollaoglu, T. G. Oliver and M. L. Sos, Family matters: How MYC family oncogenes impact small cell lung cancer, *Cell Cycle*, 2017, **16**, 1489–1498, DOI: 10.1080/15384101.2017.1339849.
76 M. Elbadawy, T. Usui, H. Yamawaki and K. Sasaki, Emerging roles of C-myc in cancer stem cell-related signaling and resistance to cancer chemotherapy: A potential therapeutic target against colorectal cancer, *Int. J. Mol. Sci.*, 2019, **20**, DOI: 10.3390/ijms20092340.
77 B. Shamloo and S. Usluer, p21 in cancer research, *Cancers*, 2019, **11**(8), 1178.
78 L. Xiao, Y. Wang, W. Liang, L. Liu, N. Pan, H. Deng, L. Li, C. Zou, F. Leung and Y. Zhou, LRH-1 drives hepatocellular carcinoma partially through induction of c-myc and cyclin E1, and suppression of p21, *Cancer Manage. Res.*, 2018, **10**, 2389–2400.
79 H. Sun, M. Yin, D. Hao and Y. Shen, Anti-cancer activity of catechin against A549 lung carcinoma cells by induction of cyclin kinase inhibitor P21 and suppression of cyclin E1 and P–AKT, *Appl. Sci.*, 2020, **10**(6), 2065.
80 Y. E. Tian, H. A. N. Wan and G. Tan, Cell cycle-related kinase in carcinogenesis, *Oncol. Lett.*, 2012, **4**, 601–606.
81 X. Xia, Q. Ma, X. Li, T. Ji, P. Chen, H. Xu, K. Li, Y. Fang, D. Weng, Y. Weng, *et al.*, Cytoplasmic p21 is a potential predictor for cisplatin sensitivity in ovarian cancer, *BMC Cancer*, 2011, **11**, 399.
82 I. D. Kartika, H. Kotani, Y. Iida, A. Koyanagi, R. Tanino and M. Harada, Protective role of cytoplasmic p21Cip1/Waf1 in apoptosis of CDK4/6 inhibitor-treated senescence in breast cancer cells, *Cancer Med.*, 2022, **10**(24), 8988–8999.
83 Q. Hu and T. Huang, Regulation of the Cell Cycle by ncRNAs Affects the Efficiency of CDK4/6 Inhibition, *Int. J. Mol. Sci.*, 2023, **24**, 8939.
84 A. Fariha, I. Hami, M. I. Q. Tonmoy, S. Akter, H. Al Reza, N. M. Bahadur and M. S. Hossain, Cell cycle associated miRNAs as target and therapeutics in lung cancer treatment, *Heliyon*, 2022, **8**(10), e11081.
85 B. O'leary, R. S. Finn and N. C. Turner, Treating cancer with selective CDK4/6 inhibitors, *Nat. Rev. Clin. Oncol.*, 2016, **13**(7), 417–430.